JOURNAL OF GEOPHYSICAL RESEARCH, VOL. 97, NO. B12, PAGES 17,503–17,529, NOVEMBER 10, 1992

# Seismicity and Shape of the Subducted Nazca Plate

THOMAS CAHILL[1] AND BRYAN L. ISACKS

*Institute for the Study of Continents and Department of Geological Sciences, Cornell University, Ithaca New York*

An updated compilation of earthquake locations and focal mechanism solutions from the International Seismological Centre and Preliminary Determination of Earthquakes is the basis of a comprehensive study of the geometry of the Wadati-Benioff zone beneath western South America. The new data support previous mapping of a sharp flexure rather than a tear in the subducted Nazca plate beneath southern Peru and provide evidence for a similar flexure in the southward transition from nearly horizontal subduction to a slab with ~30° dip at latitude 33°S. In contrast, the transition from 30° slab dip beneath Bolivia to a nearly horizontal dip in the region between 28°S - 32°S is more gradual, occurring over several hundred kilometers of along-strike distance between 20°S and 32°S. This southward flattening corresponds to a broadening of a horizontal, benchlike part of the subducted plate formed between 100 and 125 km depth. The transition in continental tectonic style near 27°S-28°S, from a wide, volcanically active plateau to a narrow, nonvolcanic cordillera, appears not to be associated with the main slab flattening, which begins to the north of these latitudes, but with a more abrupt change in curvature of the subducted slab, from convex upward to concave upward, immediately below the plate boundary interface. The concept of Gaussian curvature is applied to slab bending to explain how subduction geometry is affected by the shape of the South American plate. We hypothesize that the polarity of vertical curvature in the subducting slab is governed by the orientation of lateral curvature of the plate margin. Focal mechanism solutions for intermediate and deep earthquakes are grouped by geographic region and inverted for the orientation and relative magnitudes of the principal stresses. Results of the inversion indicate that downdip extension dominates in the slab above 350 km while downdip compression dominates at greater depths.

## INTRODUCTION

Details of subduction geometry are crucial to refine models relating subduction geometry to upper-plate tectonics; this is especially true in the case of the South American Wadati-Benioff zone (WBZ), the east-dipping zone of mantle earthquakes that delineates the position and shape of the subducted Nazca plate. *Hamilton* [1969] and *Jordan et al.* [1983] and others have recognized the importance of using this active example of an ocean-continent convergence system for developing tectonic models of the late Mesozoic in the western United States. We present an updated, three-dimensional view of the WBZ beneath western South America, produced by adding 9 years of teleseismic data to previous compilations of mantle seismicity.

The feature that most strongly characterizes the subduction geometry beneath the Andean cordillera is the along-strike variation in dip of the subducted Nazca plate [*Sykes and Hayes*, 1971; *Barazangi and Isacks*, 1976; *Bevis and Isacks*, 1984]. *Barazangi and Isacks* [1976] described the subducted slab as having four 'segments' between 4°S and 45°S, with each segment distinguished from its neighbors by a significant change in the angle of dip. Beneath southern Peru and northern Chile (15°S to 27°S), and again south of 33°S, the WBZ dips moderately to the east at an angle of about 30°. Beneath northern and central Peru (8°S to 14°S) and western Argentina (28°S to 32°S) the subducted lithosphere extends eastward for hundreds of kilometers at a depth near 100 km before resuming its downward descent.

*Barazangi and Isacks* [1976] first interpreted the teleseismic locations as indicating the individual segments are bounded by tears in the subducting slab. They visualized the two shallow-dipping segments of slab having edges sharply offset from the adjoining segments by a throw that increases toward the downdip direction. *Hasegawa and Sacks* [1981] later inferred, from local seismic data gathered in the vicinity of the segment boundary beneath southern Peru, a continuous flexure of the slab rather than a tear. *Bevis* [1986] and *Bevis and Isacks* [1984] analyzed the distribution of teleseismic hypocenters using trend surface analysis and showed that it was possible to interpret every segment boundary in the region in terms of a smooth contortion rather than a tear.

Tears may exist in the vicinity of one or several of the large aseismic areas within the central Andean WBZ. However, the teleseismic hypocenters indicate such tears would not be segment-bounding faults with large vertical offset but rather would separate gaps lying within the space of the curved regional trend. Nothing short of one or more large tear-faulting focal mechanisms could establish the existence of lithosphere-scale ripping of the subducted slab; to date, no such event has been recognized within the set of central Andean WBZ earthquakes.

Associated with the changes in angle of subduction beneath western South America are changes in the regional-scale tectonic character of the overriding plate [*Barazangi and Isacks*,1976; *Jordan et al.* 1983]. A distinctive feature of central Andean geology is the spatial correlation between late Cenozoic arc volcanism, plateau formation, and steeper subduction angle. In this paper, digitized topographic and bathymetric data and an updated catalog of young volcanic centers from *Isacks* [1988] are used to detail the spatial relationships between subduction geometry, active volcanism, and the physiography of the Andean cordillera.

Along with its effect on the upper plate, the geometry of subducted Nazca plate also strongly influences deformation

---

[1]Now at Engineering Tectonics, P.A. Winston-Salem, North Carolina.



Paper Number 92JB00493.
0148-0227/92/92JB-00493$05.00

within the slab itself [*Isacks and Barazangi*, 1977; *Schneider and Sacks*, 1987]. The orientation of the stress field in descending slabs is manifested in the focal mechanism solutions for the intraplate events [*Isacks and Molnar*, 1971; *Creager and Boyd*, 1991]; within the set of South American mantle earthquakes are many that are large enough for determination of reliable fault-plane solutions. We use several previously unpublished solutions along with Harvard Centroid Moment Tensor (HCMT) solutions and those of *Stauder* [1973, 1975] to invert for the principal axes and relative magnitudes of stress in the subducted slab.

## DATA

### *Wadati-Benioff Zone Hypocenters*

The catalogs of the International Seismological Centre (ISC) for the period of 1964-1985 and the United States Geological Survey Preliminary Determination of Epicenters (PDE) for the periods of 1963 and 1986-1988 were the primary sources of data used in this study. Intermediate-depth events (h>60 km) were selected from these two catalogs on the basis of the number of arrival time reports ($n$) used to locate the earthquake.

In a study of WBZ morphology, some grading and culling of the data are necessary to assure use of only reliable hypocentral locations. We chose to employ $n$ as our sole selection criterion. Standard hypocenter grading schemes, based on the geographic distribution of teleseismic reporting stations, local station geometry, and surface-reflected phases to verify focal depths, are difficult to apply to South American WBZ earthquakes. The azimuthal and distance distribution of seismograph stations for events in this region is peculiar; there are few stations lying between $\Delta$=10° and $\Delta$=85° to the west (the eastern Pacific Ocean) and few stations between $\Delta$=10° and $\Delta$=80° to the east (the Atlantic Ocean). Poor local coverage (few stations or poor distribution with $\Delta \leq 5°$) is also common, so depth estimates from reduction of least squares of global travel time residuals is commonly poor. Furthermore, focal depth estimates provided by teleseismic *pP-P* and *sP-P* arrival time delays are of limited value because of improper identification of reflected phases [*Cahill and Isacks*, 1986] and because of anomalous velocities for both the direct P and reflected ray paths [*Kono et al.*, 1985].

Reliable teleseismic locations are typically those with greatest number of $P$ wave arrival time reports ($n$) used to locate the event. Figure 1*a* shows how the standard deviation of travel time residuals, an indicator of the reliability of hypocentral locations, decreases with increasing $n$. Both intuitively and empirically, we know that the number of station reports will increase with the magnitude of an earthquake (Figure 1*c*), and, of course, b-value studies consistently show a logarithmic decrease in the number of events above a given magnitude (Figure 1*b*). Choosing only the most reliable hypocenters, therefore, often eliminates much of the data set. The task is to set the selection criteria in such a way as to keep as much of the data as is necessary to define the shape of the subducted slab, without including many of the poorer locations that smear the image.

We observed that earthquakes with $n \geq 40$ define narrow, clustered zones in areas of intense seismicity. Locations for these events are probably good, at least relative to one another (i.e., they are precise, if not accurate). Conversely, for $n<15$ so much scatter in location occurs that a simple surface can no longer be discerned. This observation could be predicted from noting that events with $n<15$ often have a large standard deviation of travel time residuals ($s$), one indicator of location quality (Figure 1*a*).

The hypocentral data presented in the cross sections and regional seismicity maps include all events reported by 15 or more stations. In determining the best fitting depth contours, a more restrictive subset of the data was used; all hypocenters based on 40 or more ($n \geq 40$) $P$ arrival time reports were included in the selection of events used; in areas where the seismicity represented by $n \geq 40$ was sparse or nonexistent, events with fewer reports (first $25 \leq n \leq 39$, then $15 \leq n \leq 24$) were considered; these smaller events were rejected if arrival time residuals from nearby stations ($\Delta \leq 5°$) were very large.

In the course of selecting data to use for this study we considered the complete set of available teleseismic locations. In addition to the data sources mentioned above, this included the International Seismological Summary catalog between 1950 and 1963, the PDE catalog from 1950-1982, and an unpublished 1964 compilation of *Sykes and Hayes* [1971]. Comparing maps made from these data sets, which span almost 40 years, we observed that consistency in the spatial distribution of intermediate-depth seismicity is a fundamental feature of the South American WBZ. The clustering of events into tight bands of seismicity noted by *Santo* [1969] for the period of 1960-1968 and by *Stauder* [1973, 1975] for 1962-1971 is reproduced faithfully by events from other time intervals of similar length from any of the other compilations.

Furthermore, no event in the period between 1950 and 1985 has been reliably located in any of the substantial spatial gaps in seismicity that also characterize the South American WBZ. Data sets beginning in 1964, then, are more than simply representative of the entire record; hypocenters from earlier years are "redundant" in a positive sense as they demonstrate the reproducibility of the spatial patterns.

### *Topography*

The topographic data presented in the cross sections were digitized from Defense Mapping Agency Operational Navigation Chart series at a scale of 1:1,000,000 [*Isacks*, 1988] and bathymetric charts of the easternmost Pacific [*Mammerickx and Smith*, 1978]. The topographic data were digitized at 3-min. latitude and longitude intervals, producing a 20 x 20 grid of elevations for each square degree. The profiles of topography shown in the cross sections are a running average of discrete elevations in a 30-km wide swath centered on the line of projection. The locations of young volcanic centers come from *Simpkin et al.* [1981] and *Isacks* [1988]. Established ages are lacking for many volcanic centers and the classification of these structures as late Cenozoic volcanoes is based on geomorphic appearance in Landsat/Thematic Mapper images [*Isacks*, 1988].

### *Focal Mechanism Data*

Twelve previously unpublished solutions, determined by an analysis of first motions of $P$ waves and the polarization of $S$ waves on long period World-Wide Standard Seismographic Network records, twenty solutions from *Stauder* [1973, 1975], and 183 HCMT solutions comprise the focal mechanism data set. These focal mechanisms are inverted for stress orientation using the method developed by *Gephart* [1990].

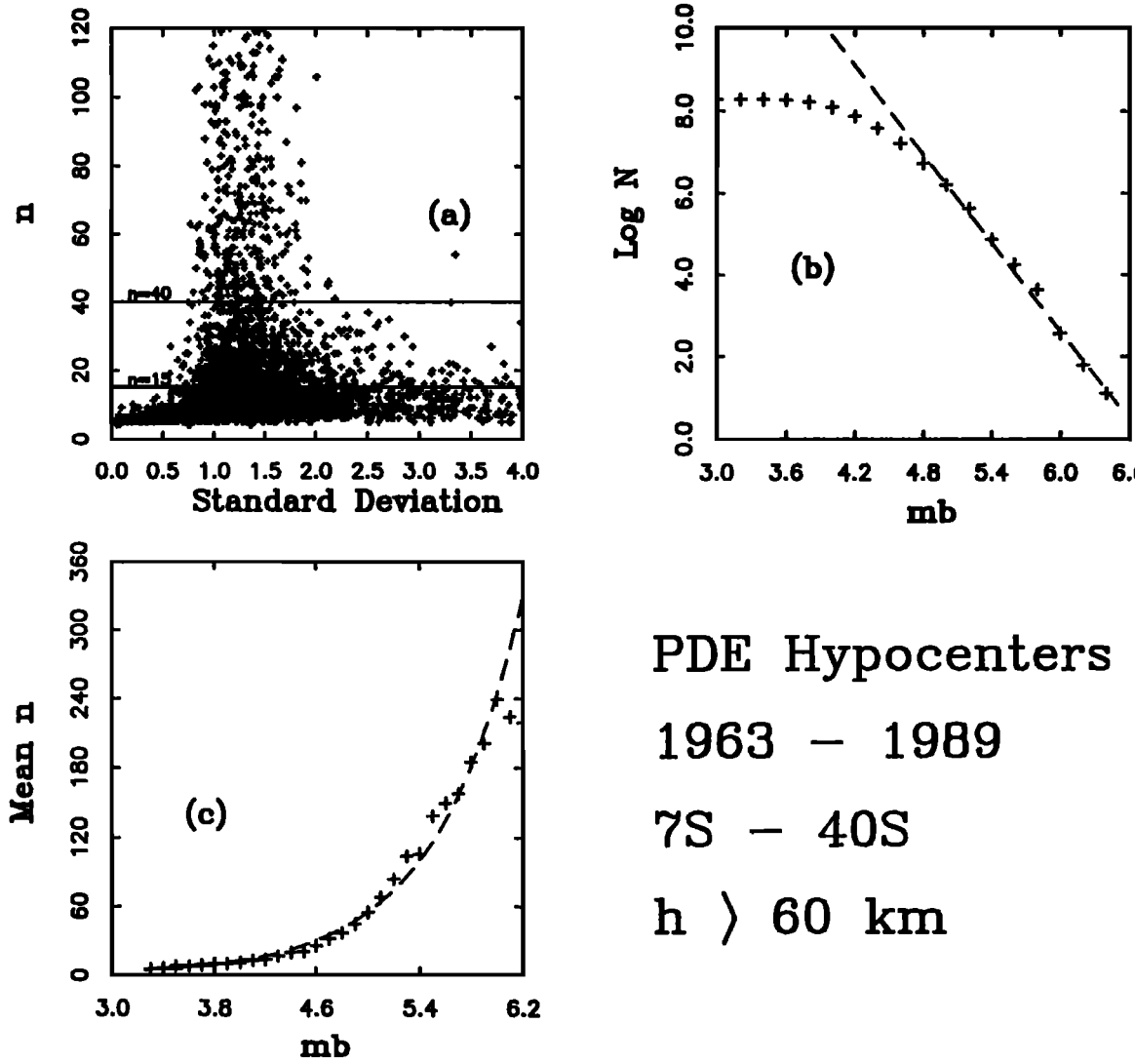


Fig. 1. Statistics illustrating the relationships between $n$, the number of $P$ wave arrivals used to locate an earthquake, quality of locations, and magnitude for intermediate-depth earthquakes beneath the central Andes. (*a*) The number of arrival times reports $n$ is plotted against the standard deviation of travel time residuals, showing that above n=40 the standard deviation is uniformly small, and that below $n$=25 the standard deviation, and usually the location, is often very large. (*b*) Demonstratio of the magnitude-frequency relationship for slab events. The curve is linear above mb=4.8, indicating that teleseismic catalogs include all events above this magnitude. (*c*) Logarithmic increase in the number of stations reporting $P$ wave arrivals with increasing magnitude.

## Shape of the Central Andean Wadati-Benioff Zone

In Figure 2, subduction geometry is depicted by contours of depth to the middle of the inclined seismic zone. The epicenters of events used to construct the depth contours are included in Figure 2*a*, so the reader may be aware of regions where contours are extrapolated across areas of sparse seismicity. The geometry of the subducted slab is in constant transition, from flat to steep or vice versa, along its entire extent beneath the central Andes. The nearly horizontal WBZ beneath northern and central Peru (8°S to 13°S) is defined by a scattered set of earthquakes at depths between 100 km and 125 km. The subducted slab extends several hundred kilometers to the east-northeast at a dip of only 5° before resuming its descent. Near 14°S there is an abrupt transition to a more steeply inclined zone. This transition has been studied by several investigators, using both teleseismic and local data and is discussed in detail along with the other transition regions later in this paper.

Continuing southward, the contours describe a slab dipping moderately (30°) to the ENE, paralleling the plate margin around the bend in the Pacific coastline (17°S to 20°S). The overall convex-up curvature of the WBZ beneath Bolivia into northern Chile and northwestern Argentina is well defined by the high level of intermediate-depth seismicity occurring in several clusters.

At about 20°S, a small horizontal "bench" forms in the slab between 100 and 125 km, manifested in Figure 2*b* by a slight increase in spacing between these depth contours. Southward from 20°S the bench widens slowly until, somewhere within the pronounced seismic gap between 25°S and 27.5°S, the shallower depth contours (50-100 km) begin to move westward toward the trench. The 125-km contour, meanwhile, continues

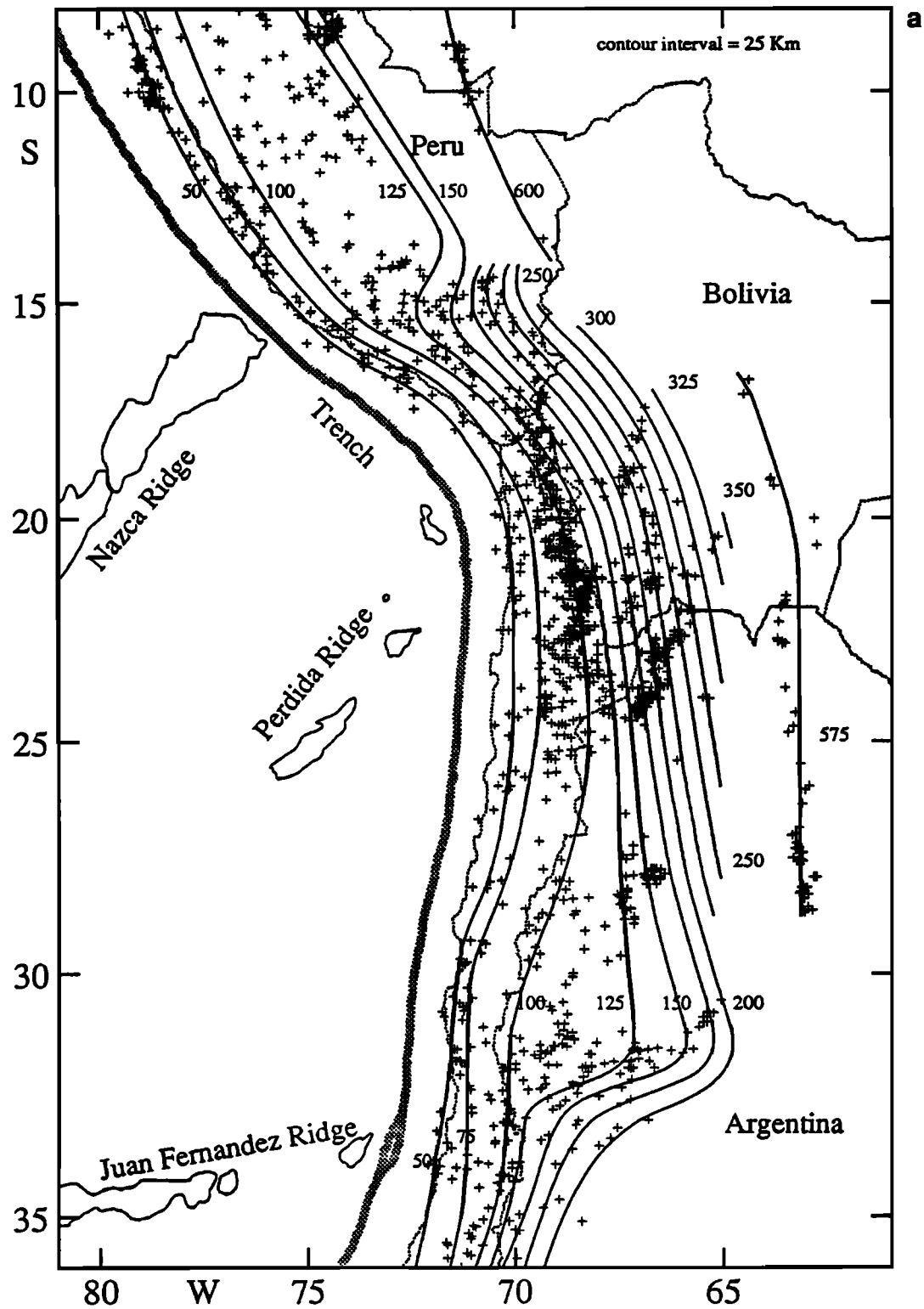


Fig. 2. (*a*) The shape of the subducted Nazca plate is shown via contours to depth of the center of the Wadati-Benioff zone; epicenters of teleseismic events used to determine the contours are shown by small crosses. To produce the contours, vertical cross sections of seismicity were taken at 100-km intervals down the entire length of the central Andean margin, points in the middle of the WBZ at 25-km depth intervals were projected onto map view, connected and smoothed. The trench axis was digitized from bathymetric charts of *Prince et al.* [1980], the 3500 m bathymetric contours were digitized from *Mammerickx and Smith*. [1978]. (b) Superimposed on the WBZ depth contours are regions of the central Andes with elevations above 3 km and locations of young volcanic centers. The association between volcanic activity, shown by solid triangles, presence of a broad plateau and contours indicating a steeper dip angle can be seen between 14°S and 27°S.

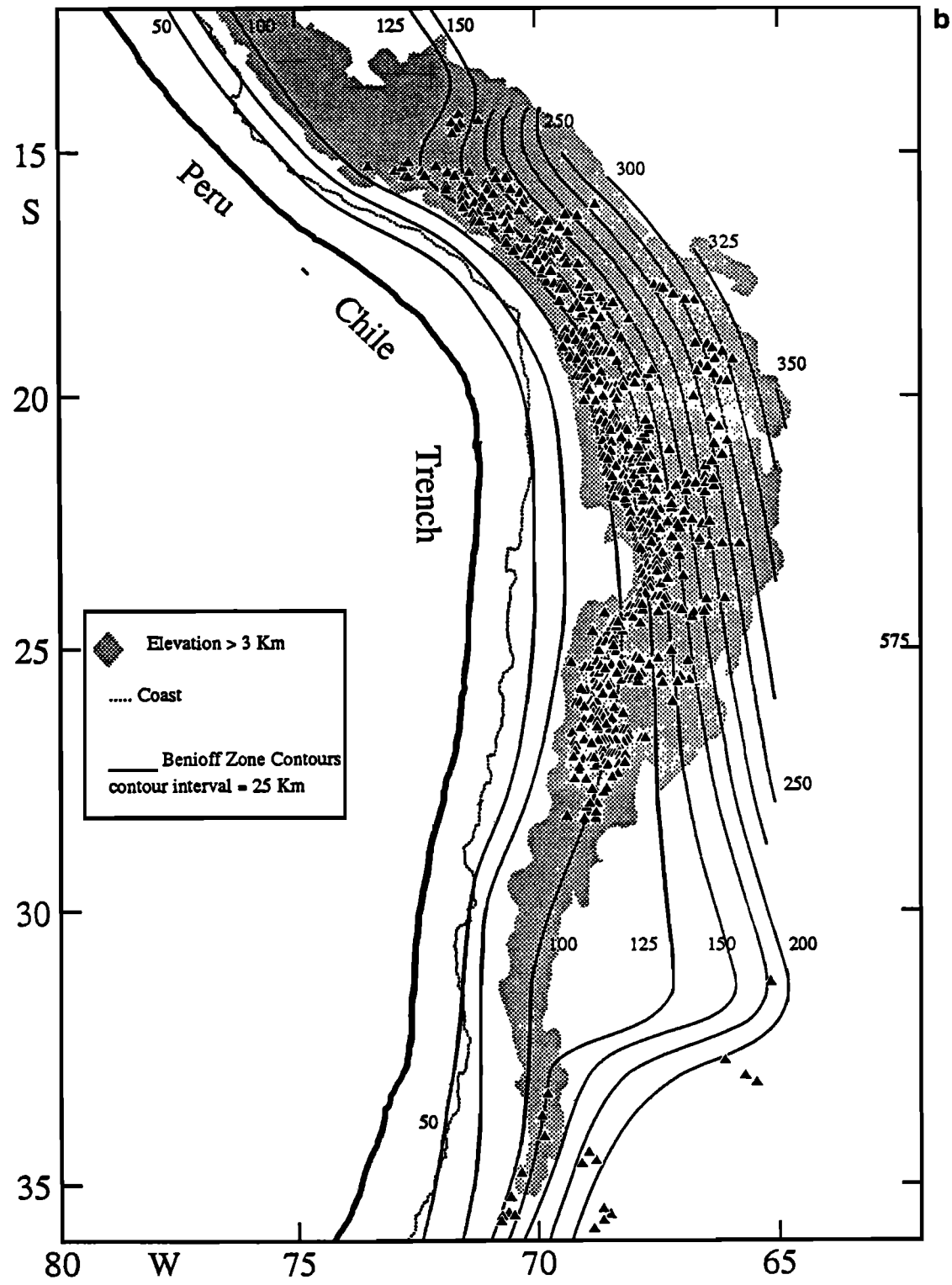


Fig. 2. (continued)

to trend toward the southeast, diverging from the plate margin. This gradual southward separation of the 100-km and 125-km depth contours illustrates further broadening of the nearly horizontal bench. Between 29°S and 32°S, the subhorizontal portion of the WBZ constitutes most of the seismically active slab.

The southern subhorizontal WBZ, like the Peruvian subhorizontal zone, exists between 100 and 125 km depth. This Argentine flat slab has been studied extensively using data collected by the seismic network of the Instituto Nacionál de Prevención Sísmica (INPRES) [*Smalley and Isacks*, 1987]. The concave-up segment between depths of 50 and 100 km, the long horizontal segment extending 300 km to the east, and the resumption of eastward descent below 125 km are all defined by abundant earthquake hypocenters.

South of 32.5°S, a major transition returns the subducted slab to the more steeply dipping orientation. The level of intermediate-depth seismic activity south of the Argentine flat

slab region drops dramatically but is nevertheless sufficient to permit a view of a short, 30°-dipping zone. Several mantle earthquakes recorded since 1979 indicate the southeast limb of the antiform, which forms the transition to this steeper zone, is steeper than envisioned by *Bevis and Isacks* [1984].

Figure 3 presents a perspective view of the WBZ, which is intended to demonstrate the three-dimensional complexity of the subducted slab. Although we continue to refer to "segmentation" of the subducted slab, the earthquake hypocenters can in fact be fit to a smooth, continuous, albeit highly contorted surface. The three-dimensional surface of Figure 3 and similar three-dimensional figures presented later were computer-generated by an interpolation and surface-drawing scheme using depth contours of Figure 2 as the basis for interpolation.

Three transitions of subduction angle beneath the central Andes will be described in greater detail: the southern Peru transition (13°S to 15°S), the northwestern Argentina transition (24°S to 28°S) and the central Chile transition (32°S to 34°S). Whether these transitions take place entirely by flexure of the plate or are discontinuous (i.e., the slab is torn, hinge-faulted, or folded over on itself) is difficult to ascertain. Broad flexures in the descending plate have been adequately documented [*Isacks and Barazangi*, 1977; *Bevis and Isacks*, 1984], yet distinguishing between sharper flexures and a tearing of the slab may be impossible, given only the record of teleseismic hypocentral locations.

Theoretical arguments for the presence of tears are based on questionable assumptions of the rheological properties of the slab. *Yamaoka et al.* [1986], for example, asserted that descending slabs beneath the South Sandwich Islands and southern Peru must be torn or folded double because, without some form of discontinuity, an inextensible spherical shell cannot assume the geometry implied by the WBZ foci. However, the assumption of perfect inextensibility of subducting lithosphere is itself dubious. *Bevis* [1986] demonstrated that a perfectly inextensible spherical cap, representing presubduction oceanic lithosphere, cannot assume the shape observed in most WBZs.

*Southern Peru Transition (13°S to 15°S)*

The northernmost of the three transitions in subducted plate geometry is observed beneath southern Peru, where the slab undergoes an abrupt transformation southward from nearly horizontal subduction to a descent of about 30°. The subducted slab is seismically active in this area, and the location and form of the WBZ here have been imaged both teleseimically and by using data from local networks. Early studies of intermediate-depth seismicity in this region by *Sykes and Hayes* [1971], *Isacks and Molnar* [1971], and *Stauder* [1975], indicated the presence of both low-angle subduction beneath southern and central Peru and a more steeply dipping zone to the south. *Barazangi and Isacks* [1979] later examined the transition between these zones by using a carefully selected set of teleseismic locations. They interpreted the sudden southward increase in slab dip beneath southern Peru as a major tear in the subducted plate, with a vertical offset resulting in the upward displacement of the slab to the north. Using microearthquake locations from this same region, *Hasegawa and Sacks* [1981] concluded that the southward steepening of the subducted lithosphere was achieved by a contortion of the plate rather than a tear. Subsequent data from other temporary seismic networks operated in the same region support this interpretation [*Grange et al.*, 1984; *Boyd et al.*, 1984]. *Bevis and Isacks* [1984] applied their technique of hypocentral trend surface analysis to both teleseismic and local data sets and concluded that surfaces generated from both data sets match the interpretation of *Hasegawa and Sacks* [1981],

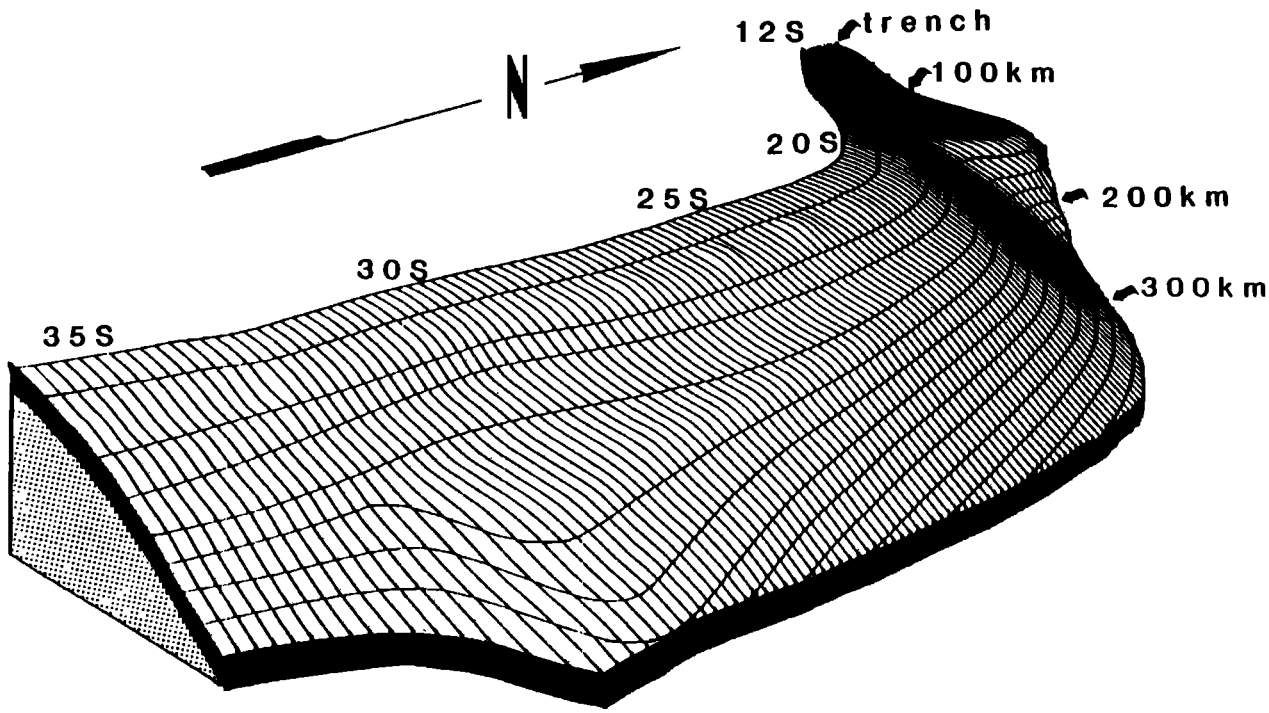


Fig. 3. A three-dimensional perspective view of the subducted Nazca plate between 36°S and 12°S. The rapid northward transition in slab dip from steep to flat at 33°S, the gradual transition from flat back to steep between 28°S and 20°S, and the second rapid transition from steep to flat at 15°S are seen.

although the lack of high-quality locations in the regions immediately to the north and northeast prohibits a definite answer to the tear versus flexure argument in this region.

The conclusion that a sharp flexure below 100 km depth results in a southward steepening of the subducted slab is supported by our updated compilation of teleseismic data. Figure 4 is an enlarged map of seismicity and depth contours for the region near the southern Peru transition. The moderately dipping WBZ south of this transition is defined by seismicity occurring in the northern end of an intense linear cluster of hypocenters beneath northern Chile and a scattering of deeper events to the east. The depth contours in this interval parallel the plate margin, smoothly wrapping around the kink in the South American coastline near 18°S.

Near 16°S, only about 100 km south of the region of horizontal subduction, the contours below 100 km depth bend abruptly to the northeast (Figure 4). The depth contours defining this flexure are controlled by many teleseismic events. The teleseismic locations support conclusions drawn from microearthquake data [*Grange et al.*, 1984; *Hasegawa and Sacks*, 1981] that the northward broadening of the area of slab lying at depths between 100 and 125 km occurs without tear faulting of the slab. However, the abrupt cessation of seismicity below 125 km depth north of 14°S prohibits any definitive statement on the nature of the deeper portion of this transition. The flexure of the descending lithosphere imaged by the WBZ seismicity here neither precludes nor proves the existence of a rip in the subducted lithosphere in the seismically inactive region immediately to the north and east.

The cross sections in Figure 5 show the abrupt northward flattening of the seismic zone and the disappearance of deeper intermediate-depth seismicity. Seismicity in the region of the central Peruvian flat slab is sparse, yet sufficiently dispersed to indicate the considerable extent of this low-angle zone, approximately 300 km in width and 1000 km in length along strike of the convergent margin. The northern limits of the flat zone are provided by clusters of earthquakes far to the north and west, near the Peru-Brazil border (8.5°S, 74°W; see Figure 2) and beneath Ecuador (2°S, 77°W). Cross sections of seismicity to the south of the transition (Figure 5, B-B' through D-D') show a simple, 30°-dipping profile.

A three-dimensional view of the southern Peru transition is presented with the interpretation of a smooth fold (Figure 6). Though the rheological and mechanical conditions determining the occurrence of throughgoing tears as opposed to folding of subducted lithosphere may be profound, the difference in the two possible geometries in this region is subtle. Discrimination between these two types of transition in southern Peru may only be achieved by obtaining precise future hypocenters in the historically quiescent area to the northeast of the recognized flexure or by the occurrence of a large slab-tearing event at the edge of this region.

*Northwestern Argentina Transition (24°S to 28°S)*

The second transition involves a change in slab geometry from the more steeply dipping zone beneath Bolivia and northern Chile to another subhorizontal zone. In contrast to the abrupt transition seen beneath southern Peru, this transition appears to occur very gradually. As with the previously discussed transition, the uncertainty with regard to the details of this transition is due in large part to the absence of intermediate-depth seismicity at a key location.

*Stauder* [1973], *Barazangi and Isacks* [1976], *Bevis and Isacks* [1984] and others described the well-developed, ENE-

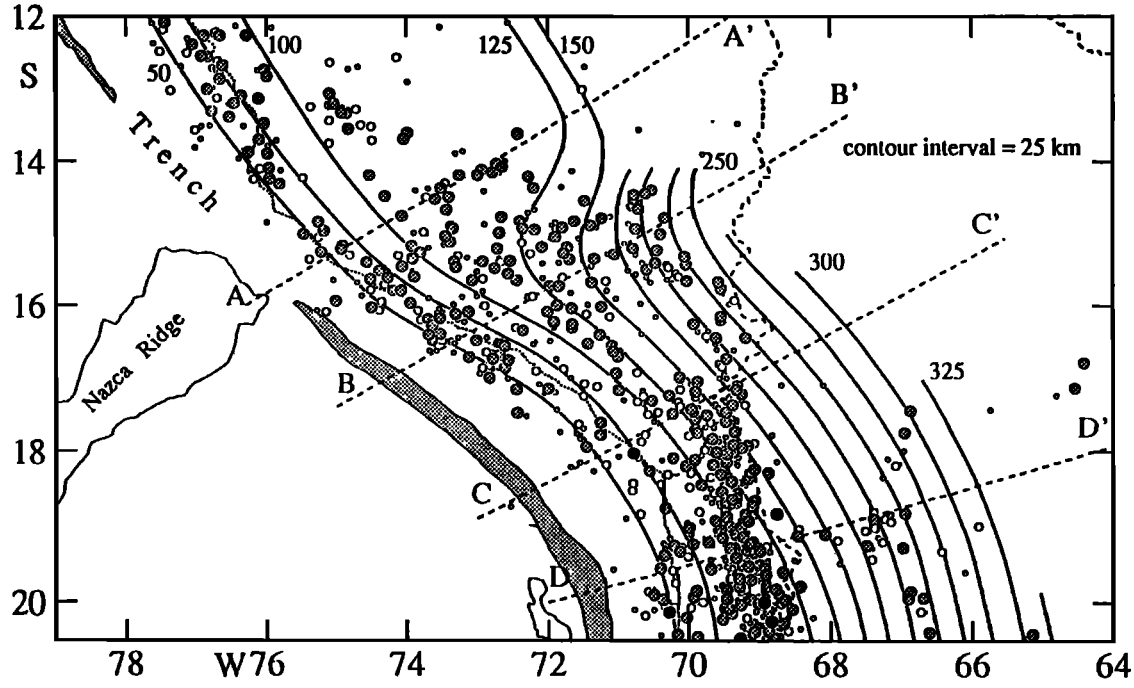


Fig. 4. Seismicity map of the southern Peru transition zone with epicenters of all earthquakes with $n \geq 15$: solid circles are epicenters of events $n \geq 40$ with independent depth control; shaded circles are epicenters of all other events with $n \geq 40$; large and small open circles show epicenters of events with $n \geq 25$ and $n \geq 15$, respectively. The northward transition from moderate to nearly horizontal subduction occurs abruptly near 15°S. The transition again occurs via a smooth contortion of the slab at depths less than 125 km, while a lack of seismicity below 150 km north of 14°S obscures the deeper nature of the transition.

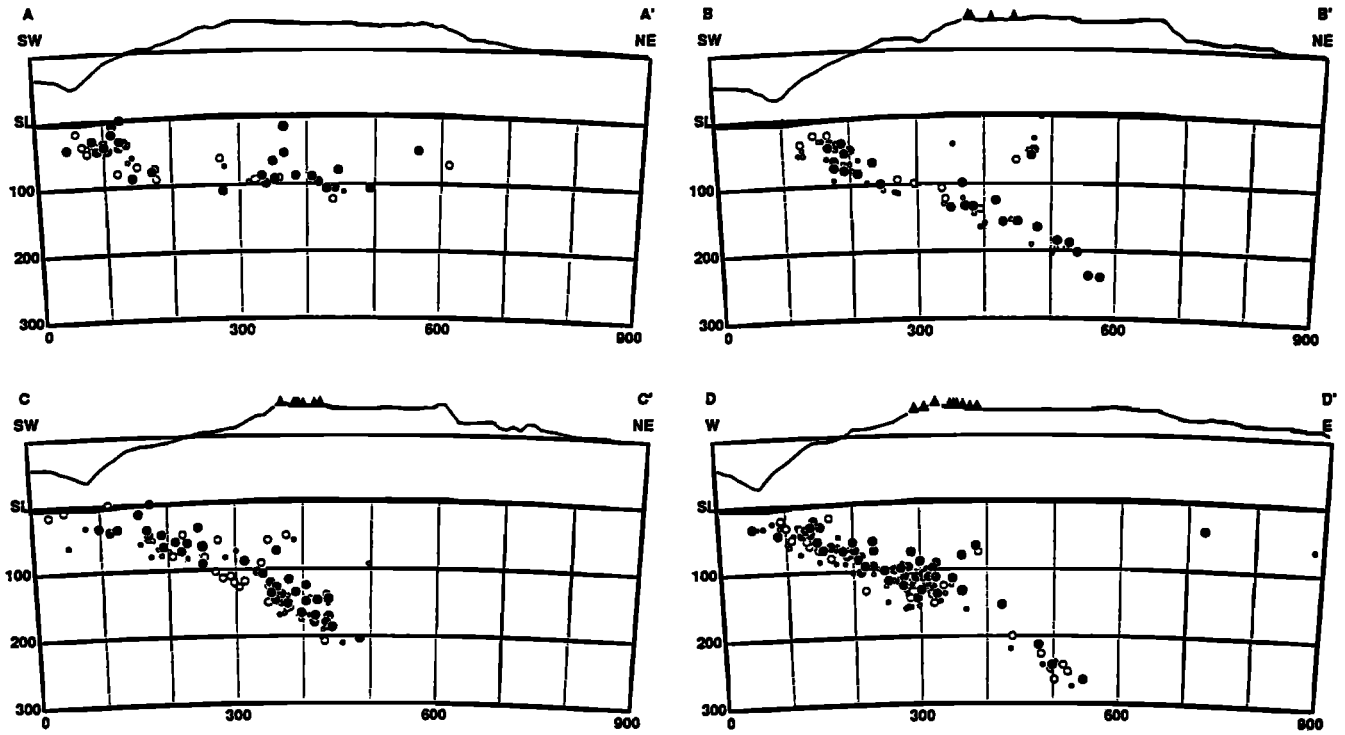


Fig. 5. Cross sections of seismicity and topography in the southern Peru transition zone. The locations of profiles A-A' through D-D' are shown in Figure 4. A broad plateau and active volcanism are seen in sections B-B' through D-D', above the steeper part of the slab. Section A-A' shows the subducted slab flattening and the accompanying disappearance of both the plateau and arc volcanics.

dipping zone of seismicity that extends southward from 15°S around the bend in the coastline of western South America. The segment 'boundary', separating the moderately dipping zone from the flattened zone beneath western Argentina, lies somewhere within the large, seismically quiescent region from 25.5°S to 27.5°S. The absence of intermediate-depth seismicity in this area has prompted opposing views regarding the nature of the "steep-to-flat" transition. *Chinn et al.* [1980] found that paths allowing propagation of high-frequency shear waves exist between most intermediate-depth earthquakes in this region and seismograph stations to the west. They concluded that this energy travels in the high Q descending slab and that no evidence exists for a large disruption in this waveguide above a depth of 200-300 km. Without generating any large or systematic residuals, *Bevis and Isacks* [1984] were able to fit the intermediate-depth hypocenters in this region with a smooth eastward-plunging anticline, whose northern limb represents the region of diminished seismic activity. *Febrer et al.* [1982], on the other hand, interpreted magnetotelluric data as indicating that the slab between 25°S and 27°S has been completely detached from the remainder of the sinking plate. They concluded that high conductivity material, presumably hot asthenosphere, rises to within 8-12 km of the surface.

The clusters of seismicity defining the WBZ in this region can be seen in the enlarged seismicity map of the central transition region (Figure 7). Earthquakes between 80 - 130 km depth are concentrated within two zones, one roughly paralleling the trench between 20°S and 25°S in northern Chile, the other being the subhorizontal zone of events beneath San Juan, Argentina (31° to 32°S). Deeper events are clustered in two separate regions: a double nest located near the western Argentina-Bolivia border (22°S to 25°S) and one

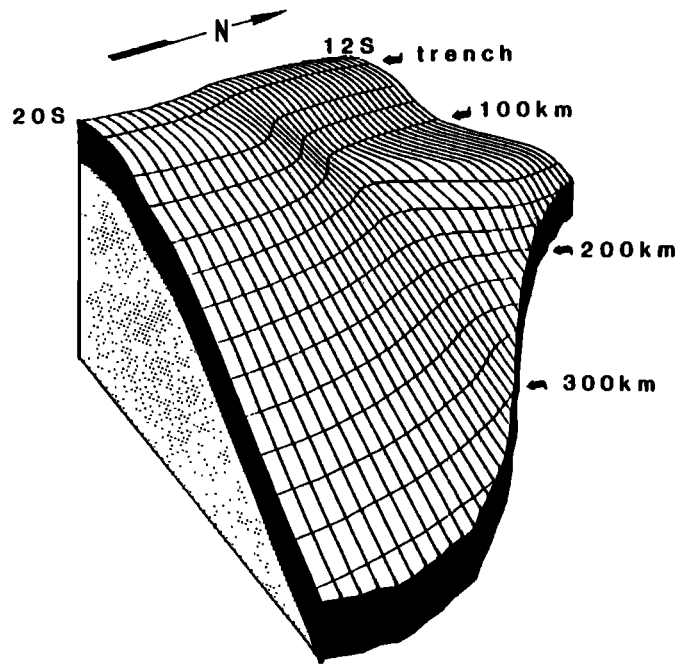


Fig. 6. A three-dimensional view from the southeast of the subducted slab between 20°S and 12°S. The abrupt northward transition in slab dip from steep to flat is shown as a smooth, tight contortion. One result of the flattening is that room no longer exists between the subducting and overriding plates for any asthenospheric material.

beneath the Pipanaco Basin in northwestern Argentina (28°S - 29°S). The gaps in seismicity between 25.5°S and 27.5°S and between 29°S and 31°S have persisted for as long as reliable locations have been available.

The characteristic feature of this central transition in slab

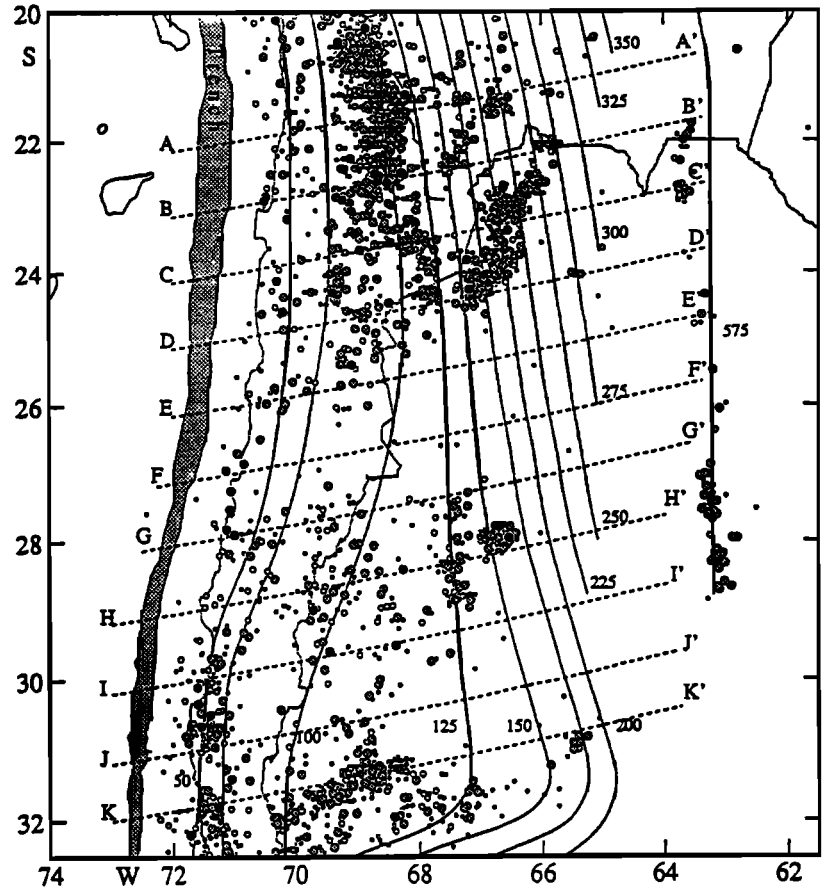


Fig. 7. Seismicity map of the northwestern Argentina transition zone. Epicenters of all earthquakes with $n \geq 15$ are shown as in Figure 4. The transition from moderate to nearly horizontal subduction occurs gradually as the longitudinal width of the 100 km deep bench expands southward. Shallower contours, meanwhile, migrate westward as the geometry of the upper part of the WBZ change from convex-up to concave-up near 28°S.

geometry is that it occurs over a great distance along strike beneath the Andean cordillera. The lack of well-located events below 100 km between 25.5°S and 27.5°S prevents any definitive conclusion about geometry of the slab in this region; we prefer the gradual transition because it is the simplest interpretation that agrees with all available data.

Figures 7 and 8 detail the distribution of events within the northwestern Argentina transition region. The southward flattening of the slab begins as a subtle inflection in the downdip arc of the slab just below 100 km depth that can be seen as far north as 22°S, beneath southern Bolivia (Figure 8 A-A'). Concomitant with this inflection, a small horizontal bench appears. The 100-km-deep horizontal bench broadens slowly between 23°S and 26°S as the inflection tightens and migrates westward toward the trench (Figure 8, B-B' through D-D'). The contours connecting hypocenters at depths of 125 km and greater meanwhile trend S-SE, diverging slowly from the plate margin.

To the south of the active moderately dipping zone, cross sections E-E' and G-G' in Figure 8, show a diminished level of intraplate, intermediate-depth activity. These sections bracket the large gap in intermediate-depth seismicity between 25.5°S and 27.5°S. Since 1963, only five events, all recorded at fewer than 25 global seismograph network stations and none having good hypocentral depth control, have been assigned locations within this large, wedge-shaped zone. Nevertheless, we interpret the slab as being continuous through this zone on the basis of the contour trends adjacent to the gap: the trends of the 125-km, 150-km and 175-km depth contours, precisely defined by the seismic activity north of this gap, extend smoothly to intersect clusters lying to the south of the gap at the appropriate depths. Neither a change in strike nor lateral offset of the contours is needed to fit the hypocentral data.

The fanning of the flattened portion of the seismic zone proceeds south of 27°S as the contours shallower than 100 km swing more rapidly toward the plate margin (Figure 7). The westward migration of the 50-km and 75-km contours, just below the zone of interplate seismicity, steepens the gradient between the trench and 100-km depth contours. The steepening gradient in this area is an accommodation of the change in slab geometry from convex-up to concave-up, to the west and east, respectively, of the westward migrating inflection. With the reappearance of relatively dense seismicity between 28°S and 29°S (Figure 8 H-H'), the horizontal bench has become the dominant feature of the intermediate-depth seismic zone. The widening of the subhorizontal portion of the WBZ continues southward to 31.5°S. Here the 100-km contours makes its closest approach to the trench axis, and the flattened bench extends for over 300 km to the east before resuming its descent (Figure 8 K-K'). A three-dimensional view (Figure 9) illustrates the interpretation of the northwestern Argentina transition as a smooth, gradual change from a 25°-30° dipping zone in the north to a doubly bent zone with a large horizontal bench in the south.

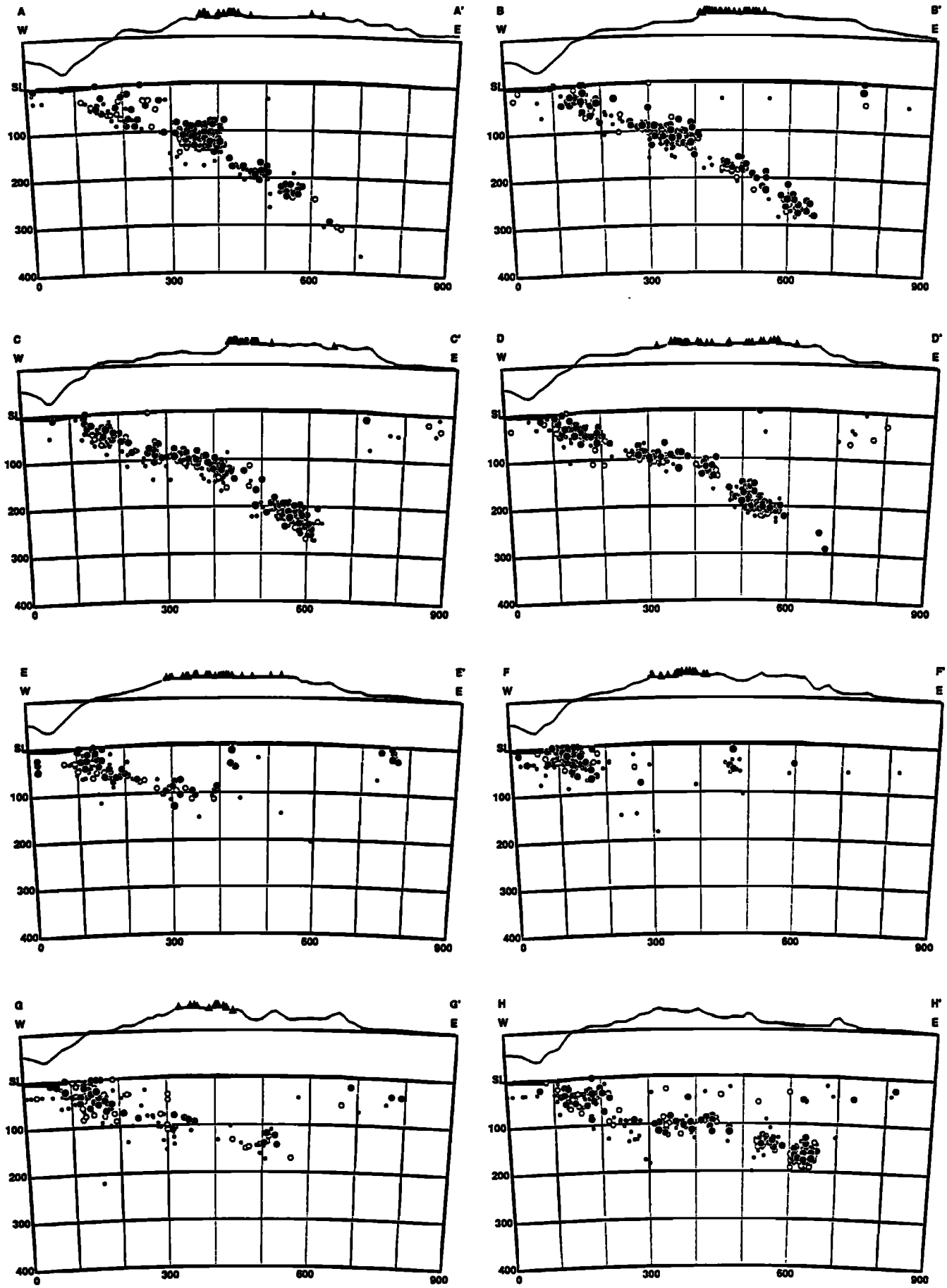


Fig. 8. Cross sections of seismicity and topography in the northwestern Argentina transition zone. The locations of profiles A-A' through K-K' are shown in Figure 7. The presence of both a broad plateau above 3.5 km and volcanic centers in sections A-A' through G-G' are found above the steeper part of the subducted slab. In sections H-H' through K-K' the plateau narrows, and volcanic centers vanish as the plate geometry flattens.

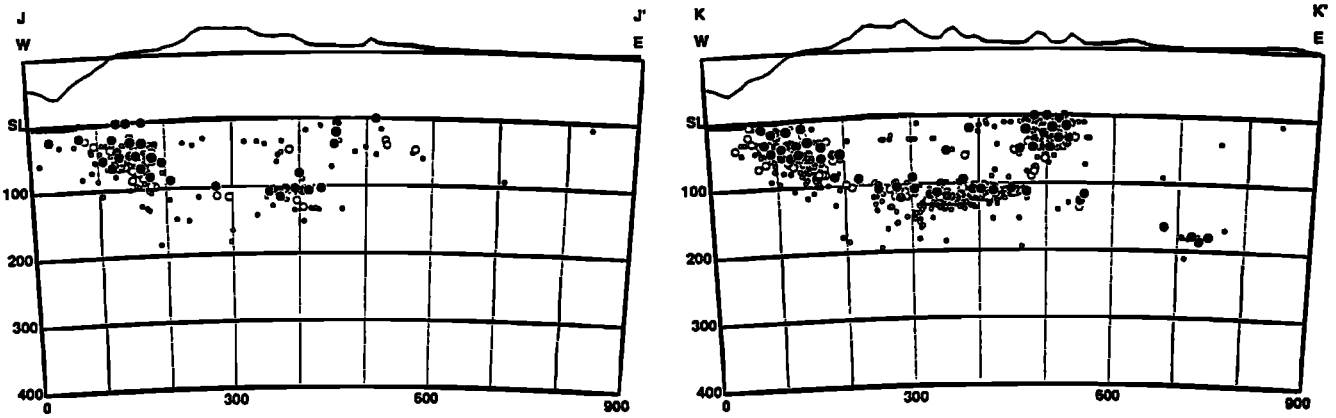


Fig. 8. (continued)

*Central Chile Transition (32°S to 34°S)*

Beneath western Argentina, immediately south of San Juan province, the downdip profile of the subducted Nazca plate once again changes rapidly. The precise nature of the southern transition historically has been difficult to detail because of a drop in the level of intermediate-depth seismicity south of the San Juan flat seismic zone. Early investigators [e.g., *Stauder*, 1973; *Santo*, 1969] did not recognize a distinct change in slab dip in this region. *Barazangi and Isacks* [1976], using thinner cross-sectional slices and a carefully selected set of hypocenters, observed a transition from low-angle subduction to an ill-defined but seemingly steeper zone to the south. They noted that the transition in slab dip coincided spatially with the intersection of the Juan Fernandez seamount chain at the Chile trench near 33°S and suggested that weak oceanic lithosphere near the Juan Fernandez seamounts might provide a linear zone along which the subducted slab could be torn.

Using a spherical surface harmonic expansion technique, *Bevis and Isacks* [1984] fit surfaces to two sets of teleseismic locations, PDE hypocenters for the period 1962-1979 and ISC hypocenters from 1964-1978. While not ruling out the existence of a tear, they found that the hypocenters in the region near 33°S could be made to fall on a simple, gently folded surface. One reason for the continued ambiguity regarding the continuity of the subducted slab was the quiescence of the deeper portions ($h$ > 125 km) of the subducted slab.

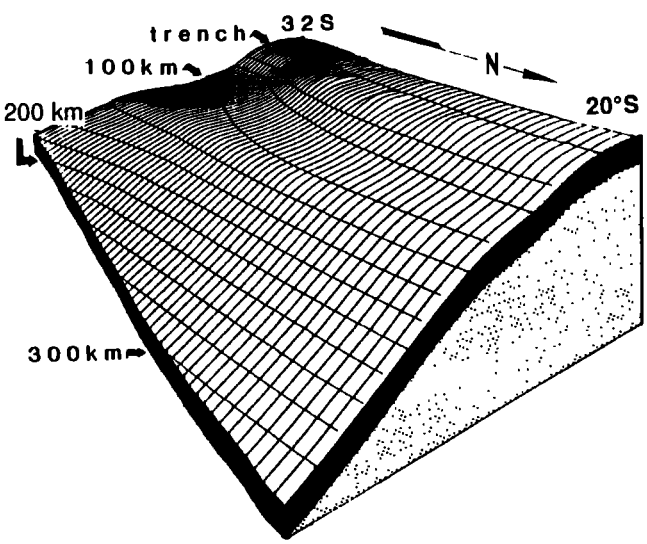


Fig. 9. A three-dimensional view from the northeast of the subducted slab between 32°S and 20°S. As a result of the gradual northward transition in slab dip from flat to steep, hot asthenospheric material fills the space between the subducting and overriding plates. The Altiplano-Puna plateau, arc magmatism and increased crustal shortening are all thought to be related to thermal weakening of the South American lithosphere [*Isacks*, 1988].

Several intermediate-depth events have occurred since 1979 on both sides of this transition. Although we still cannot rule out the possibility of a tear in the slab, we can now constrain any contortion in this area to be tighter than previously envisioned. The seismicity and contours of depth to the WBZ for the southern transition region are enlarged in Figure 10. The 50-km, 75-km and 100-km contours are well controlled by teleseismic locations; all three roughly parallel the plate margin in the region between 30°S and 35°S. The 50-km and 75-km contours are, however, more closely spaced north of 32°S where a downdip flexure is required to produce the horizontal bench observed farther to the east. The 125-km contour gradually diverges from the shallower contours in the northern part of Figure 10. Between 31.5° and 32.5°S the 125 km contour is controlled teleseismically by a tight grouping of events in the region of transition and by locations of small events located by *Smalley and Isacks* [1987] using data from a local network. We use both data sets to conclude that the 125-km contour is continuous through the region of transition south of 32°S.

No local control exists for the deeper contours because of their greater distance from the local network, and the position of these contours is estimated from events located on either side of the transition. Teleseismic locations of 37 recent (post-1979, $n$>15) earthquakes force the deeper contours to the east at the northern end of the gap and to the west at the southern end, and it is now clear that if a tearing of the lithosphere occurs in this area, it does not extend updip of the 150-km depth contour.

Figure 11 shows a pair of 70-km-wide cross sections taken immediately on either side of the transition. Cross section A-A' of Figure 11 is taken through the most seismically active portion of the Argentine flat slab. The westernmost of the earthquake foci form a convex-up curve as the subducted plate is forced down at the plate margin. Farther east, beneath the main cordillera, the zone is concave-up as the plate flexes into the 300-km-long subhorizontal zone of seismicity beneath western Argentina. Between these two zones, near the inflection from convex-up to concave-up is a 50-75-km-wide

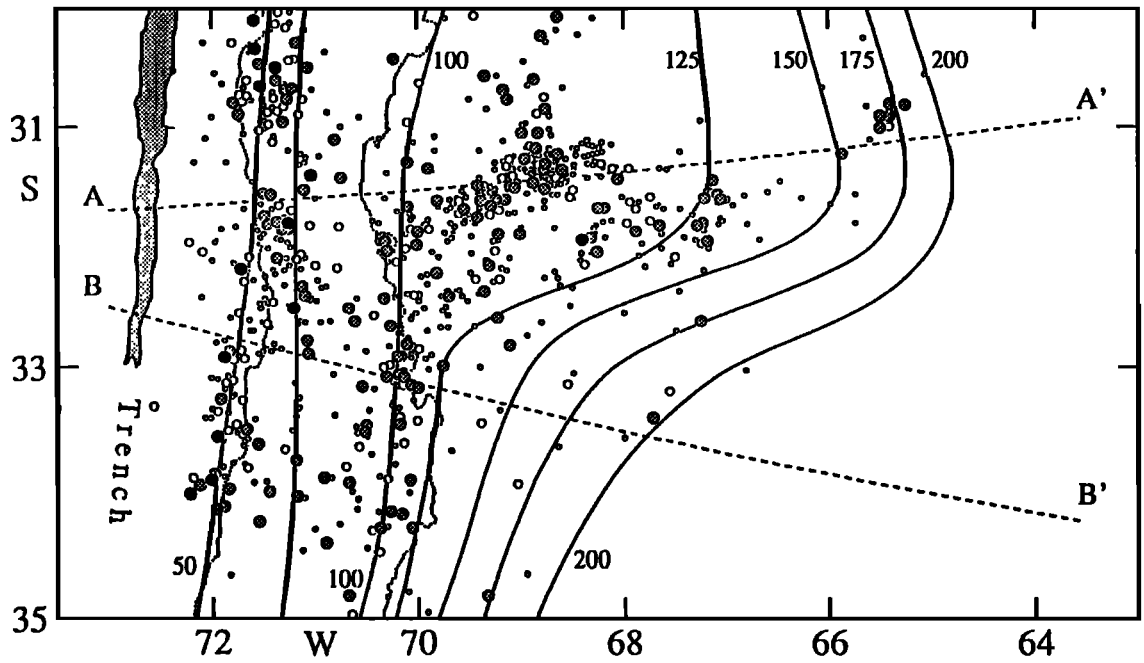


Fig. 10. Seismicity map of the central Chile transition zone. Epicenters of all earthquakes with $n \geq 15$ are shown. The southward transition from nearly horizontal subduction to subduction at ~30° dip appears to occur via a smooth contortion of the slab at depths less than 125 km. A lack of seismicity below 150 km between 32°S and 33°S obscures the nature of the transition at deeper levels.

zone of low seismicity. The deeper position of the small events lying to the west of the INPRES network has been explained by *Smalley and Isacks* [1987] as being due to mislocations resulting from a westward dip in the Moho not accounted for in the applied velocity model. Several deeper events located to the east of the flattened seismic zone indicate the slab eventually resumes its descent at a steeper angle.

Cross section B-B' shows the much simpler if less well-defined structure south of the transition. Twenty intermediate-depth events ($n$>15, $h$>100 km) between 34°S and 36°S, two of which appear on this section, occurred after 1979 helping to refine previous estimates of the location and shape of the subducted slab in this area. The WBZ between 33°S and 37°S can now be confidently described as a short 25°-dipping plane.

Figure 12 shows two three-dimensional views of possible shapes of the subducted slab in the region of the southern transition. Interpretations include a tightly contorted slab (Figure 12a), and a torn slab (Figure 12b), both drawn without vertical exaggeration. An important consequence of the rapid change in slab dip can be seen in these three-dimensional views. The shallower inflection in the slab that results in the flattening of subduction, between the 50 km and 100 km depth, disappears south of the transition. Space for mantle material above the descending plate, therefore, is available closer to the trench south of the transition, where subduction is steeper.

## CENTRAL ANDEAN TECTONICS

Associated with the changes in the angle of subduction beneath western South America are changes in the regional-scale tectonics of the overriding plate [*Barazangi and Isacks*, 1976; *Jordan et al.*, 1983]. Among the primary features listed by *Jordan et al.* [1983] as characterizing the upper plate tectonics in the region of steeper subduction (15°S to 28°S) are (1) the

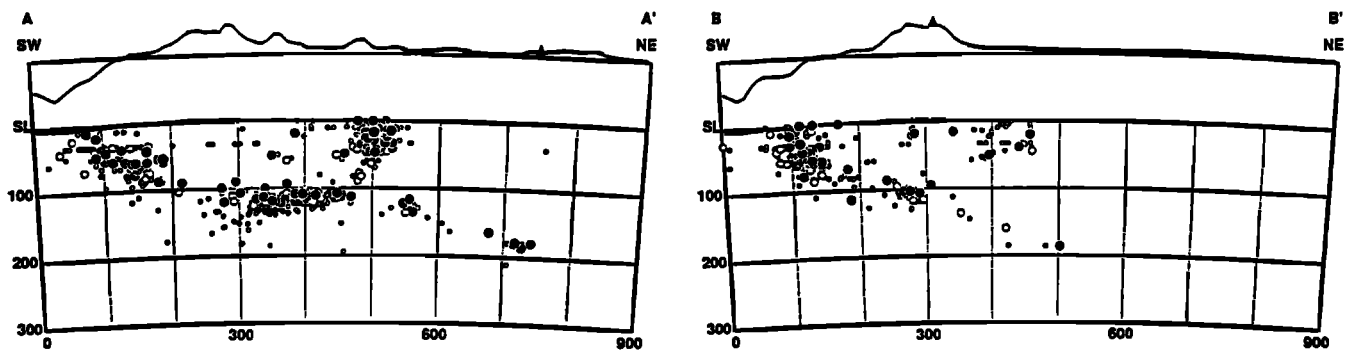


Fig. 11. Cross sections through seismicity on either side of the central Chile transition zone. Topographic profiles were generated by taking 30 km wide swath averages through a digital terrain model [*Isacks*, 1988] and are shown at both 1:1 and 10:1 vertical exaggeration. The location of Neogene volcanic centers are shown as solid triangles superimposed on the 10:1 topography. The locations of profiles A-A' and B-B' are shown in Figure 10. Foci in the WBZ between 50 and 100 km depth form a concave-up flexure that results in the subhorizontal WBZ beneath San Juan province. Sparse seismicity south of the transition defines a 30° E-dipping WBZ.

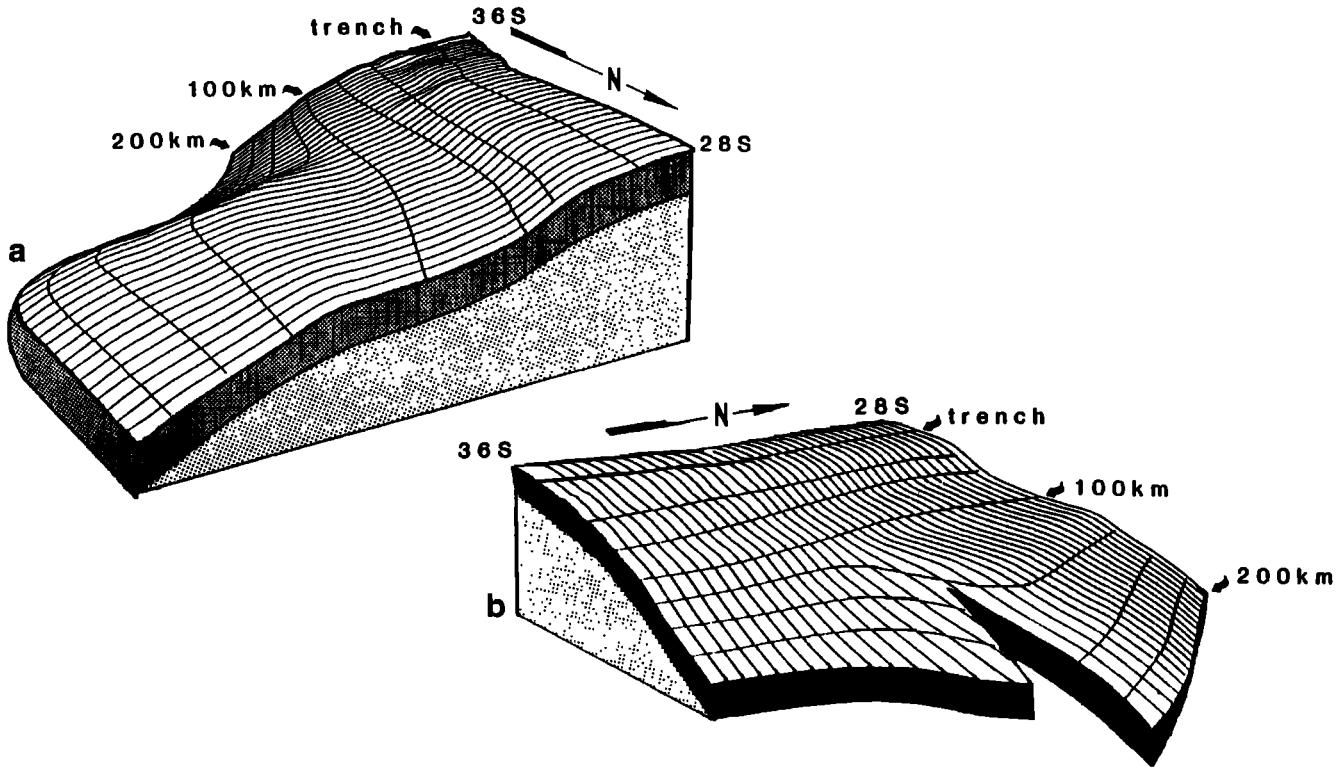


Fig. 12. Three-dimensional views of the subducted slab between 28°S and 36°S. The rapid northward transition in slab dip from steep to flat near 33°S is shown as both (*a*) a smooth contortion and (*b*) as a tear below 150 km.

existence of a broad plateau, (2) the presence of an active volcanic arc, and (3) the formation of a thin-skinned foreland thrust belt along the eastern margin of the plateau. Above the regions of low-angle subduction, neither plateaus nor active volcanoes are present, and in the southern flat-slab region (28°S to 33°S) deformation in the foreland is dominated by thick-skinned, Laramide-style structures.

In southern Peru and northern Chile the volcanic arc forms the western border of an extensive plateau, the Altiplano-Puna, which is itself dotted with young volcanoes [*Isacks*,1988]. The volcanic arc in the region overlying the flat WBZ of central Chile-western Argentina (28°S to 33°S) appears to have been extinguished between 12 and 6 Ma [*Kay et al.*, 1987]. At about the same time, between 11 Ma and 8 Ma, a final intense episode of volcanism in central Peru preceded the end of arc volcanism over what is now the northern subhorizontal zone [*Noble and McKee*, 1977].

The spatial and temporal association of volcanoes and plateaus with steeper subduction suggests that variation in dip angle affects both magma genesis and the transfer of heat upward through the South American lithosphere. Both *Kadinsky-Cade* [1985] and *Isacks* [1988] noted the parallelism of the bottom of the interplate contact zone, marked roughly by the position of the 75-km contour, and the western edge of the main cordillera, marked roughly by the 3-km elevation contour (Figure 2*b*). *Isacks* [1988] proposed that this relationship reflects the fact that the position of the western slope of the main cordillera closely follows the western tip of an asthenospheric wedge overlying the subducting Nazca plate. The presence of the wedge beneath the South American lithosphere is presumed to govern the processes of magma generation, thermal thinning, and mechanical weakening of the the overriding plate. The degree of heating and magma transfer must affect the material properties of the continental lithosphere and, therefore, play a large part in determining the style, degree, and distribution of deformation observed at the surface.

In this latitude range, many young basaltic cones are observed on the Puna surface far to the east of the main magmatic arc [*Turner and Mendez*, 1979]. Though the interpretation of *Febrer et al.* [1982] of asthenospheric material within 8-12 km of the surface in this region seems suspect, the geochemistry of Late Cenozoic basaltic volcanism in the southern Puna does suggest a mantle source with little or no slab component or crustal contamination [Knox et al., 1987]. Given the distribution of WBZ hypocenters, it is ironic that the transition that appears to be least contorted has the only independent suggestion of a tear in the slab. The plateau is considered by *Isacks* [1988] to be a primary geophysical signal of the thermal processes acting at depth, and it is well developed from 14°S to 27°S, corresponding closely to the region of steeper subduction.

The third feature of tectonic segmentation of the upper plate is found in the structural style of central Andean foreland. *Jordan et al.* [1983] noted that foreland deformation above the flat slab (28°S to 33°S) is dominated by block uplift of crystalline basement along reverse faults of varying vergence, while foreland deformation above the the steeper slab (15°S to 27°S) takes place within an eastwardly migrating classical thin-skinned fold and thrust belt. *Allmendinger et al.* [1983] suggested that this along-strike change in structural style may be related to the paleogeography of the region, specifically to the presence or absence of deep Paleozoic and Mesozoic sedimentary basins.

Regardless of the causes, it seems clear that the differing style of deformation in the foreland has resulted in considerable along-strike variation in the total crustal shortening. In a model that accounts for the modern shape of the South American

convergent plate margin, *Isacks* [1988] presented the idea that variable shortening in the Andean foreland implies a change in the plate margin shape. This change in plate margin shape, in turn, implies differential subduction rates along the margin. The total convergence rate between the Nazca plate and South American plate is the sum of subduction and shortening rates. In other words, the rate of shortening of the deformed portions of the upper plate must be subtracted from the plate convergence rate in order to establish the true rate of subduction.

Estimates of crustal shortening range from 150-170 km above the southern flat slab at 30°S [*Allmendinger et al.*, 1990] to 210-350 km in the region of steeper subduction near 18°S [*Sheffels*, 1988; *Roeder*, 1988; *Lyon-Caen et al.*, 1985]. Unfortunately, it is difficult to determine precisely the duration of the shortening episodes, and thus it is difficult to estimate accurately the magnitude of the effect of shortening on the variation of subduction rate. For example, *Allmendinger et al.* [1990] estimated 95 km of shortening above the southern flat slab since 10 Ma, and another 40-60 km of shortening between 11 and 16 Ma; meanwhile, the 210-350 km of crustal shortening in the Bolivian foreland can only be constrained as having occurred in post-Oligocene time [*Sheffels*, 1988]. If, as is within the range of possibilities, 350 km of shortening took place within the Bolivian foreland within the last 10 Ma, the subduction rate differs significantly (by 2.6 cm/yr) between 18°S and 30°S. If, however, the total amount of Bolivian foreland shortening is closer to 210 km and/or was more evenly distributed through the past 24 Ma, the difference in subduction rate along strike was negligible.

## State of Stress in the Subducting Slab

Focal mechanisms of WBZ earthquakes are the best indicator of the stress orientation within a subducting slab. *Isacks and Molnar* [1971] showed that *P* and *T* axes for intermediate and deep earthquakes within WBZs are closely aligned with the regional dip of the descending plate. In particular, they noted that *P* axes of deep earthquakes (h>350 km) are usually oriented downdip, whereas either the *T* axes or *P* axes of intermediate-depth events are oriented downdip, depending on the continuity of the WBZ. These observations, based on a global study of the relatively few available solutions for mantle earthquakes, have been confirmed by subsequent, more detailed studies of the focal mechanisms in the South American WBZ [e.g., *Stauder* 1973, 1975; *Apperson and Frohlich*, 1987]. In this study an updated compilation of focal mechanisms beneath the central Andes (Tables 1 and 2) and an inversion method is used to determine the orientation of the principal stresses within the descending plate. Included in the data set are 20 focal mechanisms from *Stauder* [1973, 1975], 183 of the HCMT solutions and 12 previously unpublished solutions, of our own.

### *Inversion Method*

In analyzing these data we employed the inversion method of *Gephart* [1990] to solve for the stress field that best fits the focal mechanisms of specified portions of the South American WBZ. The resolved shear stress on any of the WBZ slip planes is assumed to coincide with the direction of coseismic slip and can be described by four stress parameters: the three principal stress directions and one measure of the relative stress magnitudes. The inversion minimizes the discrepancies between the observed slip directions and the shear stress along the various faults, thereby finding the set of principal stresses most compatible with the entire set of fault-plane solutions.

The inversion method is, in general, a more reliable indicator of the stress field than simple compilations of *P* and *T* axes. This is because in regions having preexisting planes of weakness, the orientation of *P* and *T* axes determined for any given earthquake can deviate significantly from the $\sigma 1$ and $\sigma 3$ directions. It must be noted, however, that the validity of results from the inversion method rests heavily on a fundamental assumption: that the stresses are homogeneous over the area and time interval for any given sample. Great care was therefore taken to create subsets of the data that could reasonably be expected to satisfy this condition.

The focal mechanism solutions were separated into seven categories, based on their geographic and depth distributions. Each group contains solutions of all events from geographically small regions of the WBZ where we can reasonably expect the stresses to be homogeneous. The inversion technique was then applied separately to each group of events; the results are shown in Figure 13.

### *Southern Peru Transition Region (14°S to 16°S)*

Focal mechanism solutions have been determined for 18 intermediate-depth events in the transition region beneath southern Peru. Both *P* and *T* axes for these events show considerable variation, and though this distribution does not in itself disqualify use of the inversion method, a close look at the WBZ contours for this region (Figures 2 and 4) leads us to doubt the assumption of homogeneity of stresses. The downdip direction in the region varies in strike from 45°-105° and in dip angle from 12°-34° E-NE. We nevertheless proceeded with the inversion, obtaining a best fitting model with the least compressive stress ($\sigma 3$) at strike=60° and dip=40° (Figure 13*a*). The coincidence between the $\sigma 3$ direction and the average downdip direction once again is very good, though, for the reasons stated above, suspect. *Schneider and Sacks* [1987] used composite focal mechanism of small events within the southern Peru transition and observed that *T* axes in small discrete regions were oriented toward the contortion, that is, downdip.

### *Northern Chile Region (17°S to 24°S)*

Focal mechanisms exist for 44 intermediate-depth events in the elongate zone of seismicity beneath northern Chile. Both P and T axes for events in this region are less tightly clustered than in the NW Argentina region. Nonetheless, the T axes remain within a narrow zone, again, with the center closely approximating the downdip direction. The best fitting stress models reflect the change in strike of the slab around the Bolivian orocline. The best fitting stress model has $\sigma 3$: strike=073°, dip=12°E (Figure 13b).

### *Northwestern Argentina Region (22°S to 25°S)*

Focal mechanisms exist for 43 events in 150-300 km deep nest of events beneath northwestern Argentina. With only three exceptions the *T* axes for these events are all distributed within a moderately tight zone close to the regional downdip direction. In this portion of the WBZ the best fitting $\sigma 3$ again closely approximates the downdip direction (Figure 13c); possible solutions in this region are tightly clustered about the best fitting model, which has $\sigma 3$ where strike=080° and dip=39°E.

TABLE 1. Focal Mechanism Solutions of Intermediate-Depth Earthquakes Beneath the Central Andes

| | Date | | | Time, | Location | | | Pole 1 | | Pole 2 | | T Axis | | P Axis | | |
|---|---|---|---|---|---|---|---|---|---|---|---|---|---|---|---|---|
| | mo | day | year | UT | Latitude, deg | Longitude, deg | Depth, km | azimuth deg | plunge deg | azimuth deg | plunge deg | azimuth deg | plunge deg | azimuth deg | plunge deg | Reference |
| 1 | 3 | 13 | 77 | 2114 | -8.04 | -74.41 | 153 | 332 | 73 | 92 | 9 | 75 | 52 | 285 | 34 | H |
| 2 | 11 | 23 | 84 | 1840 | -8.16 | -76.13 | 140 | 296 | 51 | 84 | 35 | 278 | 8 | 34 | 72 | H |
| 3 | 11 | 30 | 82 | 2211 | -8.38 | -74.27 | 150 | 201 | 38 | 108 | 5 | 148 | 29 | 251 | 22 | H |
| 4 | 10 | 8 | 77 | 303 | -9.52 | -74.66 | 137 | 292 | 27 | 89 | 61 | 104 | 17 | 317 | 70 | H |
| 5 | 5 | 1 | 66 | 1622 | -8.5 | -74.3 | 165 | 279 | 15 | 157 | 63 | 251 | 54 | 117 | 27 | S2 |
| 6 | 9 | 9 | 68 | 0037 | -8.7 | -74.5 | 120 | 7 | 74 | 249 | 8 | 265 | 51 | 57 | 36 | S2 |
| 7 | 8 | 15 | 82 | 611 | -10.06 | -76.35 | 141 | 101 | 18 | 9 | 6 | 54 | 17 | 146 | 8 | H |
| 8 | 1 | 25 | 88 | 715 | -10.53 | -77.99 | 73 | 261 | 21 | 111 | 66 | 242 | 64 | 90 | 23 | H |
| 9 | 9 | 24 | 63 | 1630 | -10.6 | -78.0 | 80 | 0 | 65 | 235 | 15 | 39 | 27 | 261 | 56 | S2 |
| 10 | 3 | 2 | 83 | 707 | -11.60 | -77.83 | 79 | 249 | 12 | 3 | 63 | 49 | 29 | 277 | 51 | H |
| 11 | 6 | 15 | 79 | 853 | -12.17 | -76.66 | 77 | 261 | 21 | 126 | 62 | 232 | 61 | 96 | 22 | H |
| 12 | 1 | 26 | 84 | 1930 | -12.35 | -76.93 | 72 | 238 | 8 | 18 | 79 | 246 | 53 | 52 | 36 | H |
| 13 | 3 | 28 | 82 | 2324 | -12.77 | -76.09 | 109 | 302 | 73 | 44 | 4 | 239 | 39 | 27 | 46 | H |
| 14 | 2 | 9 | 84 | 119 | -12.90 | -76.00 | 81 | 239 | 11 | 39 | 79 | 244 | 55 | 56 | 34 | H |
| 15 | 10 | 24 | 83 | 36 | -12.96 | -76.75 | 77 | 266 | 17 | 51 | 69 | 283 | 61 | 77 | 27 | H |
| 16 | 9 | 28 | 68 | 1353 | -13.2 | -76.4 | 70 | 31 | 75 | 246 | 12 | 257 | 57 | 59 | 32 | S2 |
| 17 | 3 | 7 | 85 | 2108 | -13.82 | -72.56 | 99 | 256 | 51 | 60 | 38 | 247 | 6 | 14 | 80 | H |
| 18 | 11 | 16 | 84 | 655 | -13.90 | -76.10 | 73 | 248 | 16 | 76 | 74 | 245 | 61 | 70 | 29 | H |
| 19 | 6 | 27 | 87 | 909 | -14.13 | -76.08 | 72 | 357 | 75 | 222 | 11 | 33 | 34 | 235 | 54 | H |
| 20 | 3 | 14 | 88 | 1032 | -14.28 | -73.44 | 110 | 308 | 44 | 63 | 24 | 271 | 12 | 16 | 51 | H |
| 21 | 12 | 16 | 82 | 1407 | -14.38 | -70.67 | 201 | 212 | 38 | 22 | 51 | 28 | 6 | 246 | 82 | H |
| 22 | 9 | 15 | 82 | 2022 | -14.52 | -70.84 | 169 | 247 | 33 | 19 | 46 | 46 | 7 | 302 | 63 | H |
| 23 | 9 | 15 | 82 | 2022 | -14.53 | -70.80 | 153 | 231 | 26 | 18 | 60 | 39 | 18 | 261 | 67 | C |
| 24 | 1 | 16 | 80 | 1549 | -14.54 | -73.49 | 119 | 279 | 40 | 46 | 36 | 251 | 2 | 345 | 60 | H |
| 25 | 4 | 12 | 75 | 1533 | -14.79 | -72.66 | 108 | 160 | 72 | 302 | 14 | 131 | 30 | 287 | 58 | C |
| 26 | 4 | 27 | 74 | 0601 | -14.97 | -72.20 | 133 | 154 | 58 | 270 | 15 | 112 | 25 | 237 | 52 | C |
| 27 | 9 | 20 | 84 | 953 | -15.06 | -73.50 | 118 | 280 | 28 | 79 | 60 | 92 | 16 | 303 | 71 | H |
| 28 | 3 | 26 | 85 | 1928 | -15.16 | -71.68 | 144 | 216 | 2 | 125 | 10 | 80 | 6 | 171 | 8 | H |
| 29 | 7 | 13 | 87 | 1914 | -15.23 | -69.95 | 227 | 307 | 30 | 216 | 1 | 355 | 20 | 257 | 21 | H |
| 30 | 5 | 21 | 79 | 2222 | -15.25 | -70.09 | 233 | 278 | 77 | 11 | 1 | 358 | 44 | 204 | 43 | H |
| 31 | 12 | 31 | 77 | 753 | -15.30 | -71.68 | 161 | 230 | 3 | 134 | 62 | 74 | 36 | 204 | 42 | H |
| 32 | 5 | 21 | 79 | 2222 | -15.44 | -70.05 | 236 | 19 | 00 | 290 | 66 | 357 | 40 | 221 | 40 | C |
| 33 | 7 | 17 | 87 | 2102 | -15.48 | -74.04 | 93 | 315 | 59 | 48 | 2 | 255 | 35 | 20 | 39 | H |
| 34 | 2 | 13 | 81 | 1958 | -15.59 | -74.53 | 68 | 209 | 10 | 1 | 79 | 25 | 35 | 216 | 55 | H |
| 35 | 9 | 15 | 79 | 1002 | -15.63 | -69.56 | 231 | 173 | 75 | 24 | 13 | 35 | 57 | 198 | 31 | H |
| 36 | 3 | 13 | 87 | 1028 | -15.64 | -74.30 | 97 | 259 | 46 | 0 | 11 | 211 | 22 | 321 | 40 | H |
| 37 | 11 | 12 | 83 | 1353 | -15.73 | -74.11 | 100 | 256 | 25 | 59 | 64 | 70 | 19 | 270 | 70 | H |
| 38 | 6 | 18 | 84 | 1120 | -15.73 | -72.48 | 131 | 214 | 34 | 104 | 27 | 251 | 4 | 156 | 46 | H |
| 39 | 9 | 12 | 84 | 1917 | -15.77 | -71.89 | 150 | 221 | 44 | 52 | 46 | 47 | 1 | 149 | 85 | H |
| 40 | 6 | 17 | 70 | 0444 | -15.8 | -71.8 | 91 | 220 | 10 | 45 | 80 | 41 | 35 | 219 | 55 | S2 |
| 41 | 7 | 28 | 73 | 2218 | -16.03 | -71.26 | 110 | 77 | 40 | 336 | 14 | 18 | 38 | 122 | 17 | C |
| 42 | 1 | 22 | 78 | 2119 | -16.13 | -73.66 | 84 | 221 | 31 | 53 | 58 | 201 | 75 | 45 | 13 | H |
| 43 | 8 | 26 | 84 | 22 | -16.19 | -69.55 | 210 | 237 | 15 | 85 | 74 | 63 | 30 | 226 | 59 | H |
| 44 | 11 | 30 | 81 | 1542 | -17.02 | -69.85 | 144 | 241 | 2 | 3 | 87 | 59 | 43 | 244 | 47 | H |
| 45 | 2 | 26 | 84 | 818 | -17.26 | -70.57 | 116 | 237 | 19 | 79 | 69 | 63 | 25 | 225 | 64 | H |
| 46 | 1 | 1 | 83 | 531 | -17.31 | -69.28 | 172 | 232 | 10 | 126 | 58 | 76 | 28 | 200 | 46 | H |
| 47 | 5 | 22 | 88 | 1247 | -17.36 | -69.39 | 179 | 267 | 1 | 2 | 83 | 80 | 44 | 274 | 45 | H |
| 48 | 7 | 19 | 87 | 1400 | -17.37 | -70.41 | 128 | 161 | 85 | 53 | 1 | 58 | 46 | 229 | 43 | H |
| 59 | 5 | 20 | 88 | 319 | -17.54 | -69.44 | 137 | 239 | 19 | 104 | 64 | 73 | 24 | 213 | 60 | H |
| 50 | 9 | 1 | 83 | 2001 | -17.58 | -69.98 | 105 | 229 | 13 | 53 | 77 | 50 | 32 | 228 | 58 | H |
| 51 | 2 | 6 | 88 | 1803 | -18.04 | -66.96 | 285 | 270 | 8 | 126 | 80 | 95 | 37 | 263 | 53 | H |
| 52 | 7 | 30 | 65 | 0545 | -18.1 | -70.8 | 72 | 235 | 1 | 145 | 65 | 78 | 38 | 210 | 40 | S1 |
| 53 | 2 | 26 | 88 | 231 | -18.10 | -69.67 | 146 | 248 | 18 | 99 | 70 | 76 | 26 | 233 | 61 | H |
| 54 | 10 | 3 | 87 | 335 | -18.22 | -69.31 | 137 | 226 | 7 | 129 | 44 | 79 | 24 | 188 | 35 | H |
| 55 | 2 | 25 | 83 | 2249 | -18.27 | -69.44 | 145 | 267 | 3 | 163 | 75 | 100 | 40 | 252 | 47 | H |
| 56 | 4 | 30 | 86 | 1409 | -18.35 | -69.70 | 118 | 238 | 17 | 124 | 53 | 83 | 21 | 200 | 51 | H |
| 57 | 6 | 3 | 82 | 643 | -18.89 | -68.02 | 195 | 299 | 42 | 173 | 33 | 328 | 5 | 229 | 59 | H |
| 58 | 8 | 20 | 65 | 0942 | -18.9 | -69.0 | 128 | 235 | 8 | 115 | 74 | 66 | 35 | 219 | 51 | S1 |
| 59 | 11 | 2 | 81 | 1430 | -18.91 | -69.78 | 135 | 274 | 13 | 134 | 73 | 103 | 31 | 260 | 57 | H |
| 60 | 9 | 21 | 83 | 1027 | -18.98 | -69.12 | 116 | 212 | 17 | 39 | 73 | 34 | 28 | 210 | 62 | H |
| 61 | 4 | 2 | 78 | 907 | -19.07 | -69.28 | 118 | 241 | 37 | 65 | 53 | 63 | 8 | 230 | 82 | H |
| 62 | 5 | 23 | 83 | 54 | -19.14 | -69.15 | 116 | 263 | 14 | 43 | 72 | 74 | 30 | 279 | 58 | H |
| 63 | 3 | 15 | 86 | 1129 | -19.16 | -67.46 | 241 | 289 | 31 | 169 | 40 | 137 | 5 | 235 | 55 | H |
| 64 | 8 | 8 | 87 | 1548 | -19.19 | -70.14 | 80 | 263 | 20 | 86 | 70 | 84 | 25 | 261 | 65 | H |
| 65 | 6 | 17 | 79 | 1933 | -19.20 | -68.89 | 127 | 251 | 14 | 109 | 72 | 80 | 30 | 236 | 58 | H |
| 66 | 5 | 18 | 85 | 1659 | -19.20 | -69.12 | 126 | 256 | 12 | 136 | 66 | 92 | 30 | 231 | 53 | H |

TABLE 1. (continued)

| | Date | | | Time, | Location | | | Pole 1 | | Pole 2 | | *T* Axis | | *P* Axis | | |
|---|---|---|---|---|---|---|---|---|---|---|---|---|---|---|---|---|
| | mo | day | year | UT | Latitude, deg | Longitude, deg | Depth, km | azimuth deg | plunge deg | azimuth deg | plunge deg | azimuth deg | plunge deg | azimuth deg | plunge deg | Reference |
| 67 | 5 | 26 | 80 | 1841 | -19.36 | -69.29 | 104 | 259 | 23 | 87 | 67 | 82 | 22 | 254 | 67 | H |
| 68 | 3 | 26 | 81 | 1804 | -19.37 | -68.96 | 144 | 255 | 14 | 89 | 76 | 78 | 31 | 251 | 59 | H |
| 69 | 6 | 30 | 77 | 246 | -19.40 | -69.53 | 122 | 258 | 21 | 59 | 68 | 73 | 24 | 270 | 65 | H |
| 70 | 3 | 22 | 82 | 2144 | -19.88 | -68.74 | 139 | 257 | 5 | 142 | 78 | 87 | 39 | 244 | 49 | H |
| 71 | 8 | 24 | 66 | 0717 | -19.9 | -69.1 | 100 | 240 | 5 | 140 | 63 | 82 | 34 | 214 | 43 | S1 |
| 72 | 3 | 08 | 66 | 2046 | -20.0 | -68.9 | 122 | 3 | 75 | 232 | 10 | 42 | 34 | 245 | 53 | S1 |
| 73 | 3 | 4 | 87 | 1004 | -20.03 | -68.93 | 133 | 219 | 34 | 76 | 50 | 55 | 8 | 168 | 69 | H |
| 74 | 2 | 6 | 88 | 742 | -20.17 | -68.51 | 135 | 222 | 10 | 116 | 57 | 67 | 28 | 190 | 46 | H |
| 75 | 5 | 11 | 67 | 1505 | -20.3 | -68.5 | 115 | 234 | 18 | 100 | 64 | 67 | 24 | 209 | 59 | S1 |
| 76 | 7 | 9 | 87 | 407 | -20.48 | -68.74 | 124 | 215 | 18 | 77 | 67 | 47 | 26 | 193 | 60 | H |
| 77 | 6 | 1 | 81 | 1950 | -20.49 | -65.19 | 349 | 253 | 16 | 124 | 65 | 88 | 26 | 228 | 57 | H |
| 78 | 6 | 12 | 65 | 1850 | -20.5 | -69.3 | 102 | 5 | 72 | 242 | 10 | 49 | 33 | 259 | 52 | S1 |
| 79 | 6 | 18 | 77 | 1649 | -20.89 | -68.45 | 136 | 225 | 30 | 11 | 55 | 32 | 13 | 264 | 69 | H |
| 80 | 2 | 22 | 88 | 1913 | -20.93 | -69.80 | 67 | 219 | 11 | 88 | 74 | 49 | 33 | 203 | 54 | H |
| 81 | 10 | 21 | 87 | 2325 | -21.14 | -69.69 | 76 | 235 | 18 | 110 | 61 | 73 | 24 | 204 | 56 | H |
| 82 | 2 | 20 | 86 | 916 | -21.15 | -70.11 | 92 | 270 | 29 | 64 | 58 | 80 | 15 | 301 | 71 | H |
| 83 | 12 | 27 | 67 | 0917 | -21.2 | -68.3 | 135 | 233 | 35 | 73 | 53 | 61 | 9 | 194 | 76 | S1 |
| 84 | 12 | 11 | 80 | 1815 | -21.27 | -68.15 | 121 | 275 | 35 | 69 | 52 | 84 | 9 | 319 | 74 | H |
| 85 | 4 | 14 | 80 | 2357 | -21.29 | -68.73 | 115 | 234 | 28 | 105 | 50 | 75 | 12 | 189 | 61 | H |
| 86 | 8 | 23 | 77 | 312 | -21.32 | -68.23 | 136 | 219 | 37 | 35 | 53 | 37 | 8 | 232 | 81 | H |
| 87 | 6 | 19 | 87 | 1900 | -21.37 | -68.38 | 133 | 259 | 27 | 106 | 60 | 88 | 17 | 232 | 69 | H |
| 88 | 12 | 31 | 82 | 135 | -21.39 | -68.05 | 142 | 254 | 31 | 93 | 57 | 81 | 13 | 227 | 74 | H |
| 89 | 6 | 10 | 82 | 1143 | -21.39 | -67.40 | 202 | 321 | 33 | 215 | 23 | 0 | 6 | 264 | 42 | H |
| 90 | 12 | 3 | 87 | 1104 | -21.40 | -68.26 | 125 | 255 | 35 | 91 | 54 | 82 | 9 | 221 | 78 | H |
| 91 | 8 | 10 | 79 | 128 | -21.41 | -66.61 | 252 | 251 | 16 | 93 | 73 | 76 | 29 | 243 | 60 | H |
| 92 | 8 | 27 | 85 | 1044 | -21.46 | -67.45 | 218 | 333 | 53 | 206 | 25 | 5 | 15 | 248 | 59 | H |
| 93 | 6 | 16 | 81 | 541 | -21.49 | -68.34 | 125 | 254 | 31 | 28 | 50 | 54 | 10 | 303 | 64 | H |
| 94 | 5 | 4 | 79 | 1721 | -21.56 | -68.28 | 124 | 257 | 25 | 10 | 39 | 46 | 8 | 307 | 49 | H |
| 95 | 5 | 12 | 87 | 1612 | -21.79 | -68.32 | 139 | 214 | 27 | 73 | 57 | 48 | 15 | 177 | 66 | H |
| 96 | 1 | 10 | 83 | 917 | -21.85 | -68.32 | 132 | 277 | 10 | 72 | 79 | 93 | 35 | 283 | 55 | H |
| 97 | 10 | 27 | 78 | 1006 | -21.91 | -65.79 | 300 | 263 | 19 | 44 | 66 | 71 | 24 | 285 | 61 | H |
| 98 | 6 | 16 | 80 | 545 | -22.03 | -68.47 | 118 | 276 | 46 | 78 | 43 | 267 | 2 | 7 | 81 | H |
| 99 | 6 | 8 | 77 | 1325 | -22.06 | -67.26 | 186 | 235 | 86 | 105 | 3 | 109 | 48 | 282 | 42 | H |
| 100 | 11 | 9 | 87 | 1746 | -22.07 | -69.47 | 70 | 274 | 24 | 169 | 30 | 130 | 4 | 223 | 40 | H |
| 101 | 6 | 1 | 87 | 150 | -22.27 | -68.51 | 121 | 229 | 27 | 117 | 35 | 81 | 5 | 177 | 47 | H |
| 102 | 7 | 21 | 83 | 711 | -22.30 | -68.53 | 135 | 283 | 7 | 32 | 68 | 85 | 35 | 305 | 48 | H |
| 103 | 9 | 11 | 87 | 34 | -22.32 | -68.36 | 133 | 257 | 32 | 92 | 57 | 83 | 13 | 233 | 75 | H |
| 104 | 5 | 29 | 82 | 326 | -22.35 | -68.37 | 117 | 237 | 21 | 82 | 67 | 65 | 23 | 221 | 65 | H |
| 105 | 1 | 2 | 74 | 1042 | -22.49 | -68.26 | 125 | 241 | 12 | 23 | 74 | 53 | 32 | 254 | 56 | C |
| 106 | 9 | 12 | 86 | 1039 | -22.52 | -70.20 | 109 | 279 | 25 | 117 | 64 | 105 | 20 | 264 | 69 | H |
| 107 | 2 | 1 | 73 | 0514 | -22.53 | -66.19 | 247 | 275 | 6 | 175 | 60 | 119 | 33 | 247 | 43 | C |
| 108 | 4 | 19 | 82 | 1154 | -22.60 | -66.02 | 266 | 270 | 18 | 104 | 71 | 93 | 27 | 262 | 63 | H |
| 109 | 1 | 1 | 84 | 2208 | -22.61 | -66.02 | 275 | 258 | 4 | 148 | 77 | 89 | 40 | 246 | 48 | H |
| 110 | 3 | 2 | 81 | 2119 | -22.64 | -65.99 | 274 | 215 | 86 | 77 | 3 | 80 | 48 | 254 | 42 | H |
| 111 | 7 | 18 | 81 | 1115 | -22.68 | -66.24 | 232 | 248 | 2 | 153 | 73 | 84 | 41 | 231 | 44 | H |
| 112 | 8 | 10 | 75 | 1025 | -22.73 | -66.62 | 222 | 240 | 20 | 57 | 70 | 59 | 25 | 242 | 65 | C |
| 113 | 2 | 10 | 82 | 2038 | -22.79 | -66.66 | 237 | 263 | 5 | 145 | 80 | 92 | 39 | 253 | 49 | H |
| 114 | 5 | 22 | 79 | 833 | -22.81 | -69.14 | 83 | 289 | 35 | 75 | 50 | 94 | 8 | 341 | 71 | H |
| 115 | 5 | 14 | 79 | 2304 | -22.81 | -69.13 | 72 | 286 | 27 | 93 | 63 | 102 | 18 | 298 | 71 | H |
| 116 | 12 | 11 | 84 | 2322 | -22.84 | -68.80 | 128 | 278 | 11 | 127 | 77 | 103 | 33 | 270 | 56 | H |
| 117 | 4 | 1 | 87 | 148 | -22.93 | -66.23 | 251 | 178 | 76 | 87 | 0 | 100 | 44 | 253 | 43 | H |
| 118 | 5 | 15 | 79 | 1732 | -22.94 | -69.22 | 93 | 276 | 13 | 79 | 77 | 93 | 32 | 282 | 58 | H |
| 119 | 5 | 14 | 79 | 1732 | -22.95 | -69.09 | 89 | 304 | 25 | 107 | 64 | 118 | 20 | 319 | 69 | C |
| 120 | 4 | 9 | 86 | 1810 | -22.96 | -66.67 | 218 | 246 | 2 | 107 | 87 | 68 | 43 | 243 | 47 | H |
| 121 | 2 | 15 | 83 | 2321 | -22.97 | -66.50 | 229 | 250 | 5 | 3 | 76 | 58 | 38 | 264 | 49 | H |
| 122 | 2 | 1 | 83 | 422 | -23.03 | -68.80 | 101 | 283 | 19 | 53 | 62 | 87 | 24 | 313 | 58 | H |
| 123 | 1 | 27 | 81 | 1425 | -23.03 | -68.03 | 140 | 282 | 24 | 57 | 58 | 86 | 18 | 318 | 62 | H |
| 124 | 10 | 8 | 85 | 947 | -23.05 | -66.43 | 244 | 259 | 1 | 40 | 88 | 78 | 44 | 260 | 46 | H |
| 125 | 12 | 31 | 84 | 1300 | -23.06 | -66.91 | 202 | 249 | 10 | 105 | 78 | 75 | 35 | 240 | 54 | H |
| 126 | 10 | 7 | 87 | 51 | -23.07 | -68.12 | 145 | 248 | 31 | 74 | 58 | 70 | 14 | 239 | 76 | H |
| 127 | 9 | 20 | 81 | 1048 | -23.08 | -66.63 | 231 | 335 | 67 | 203 | 16 | 10 | 27 | 226 | 58 | H |
| 128 | 8 | 15 | 87 | 934 | -23.10 | -68.57 | 134 | 229 | 36 | 114 | 30 | 263 | 4 | 168 | 50 | H |
| 129 | 4 | 15 | 77 | 2335 | -23.10 | -68.71 | 130 | 288 | 16 | 31 | 39 | 74 | 14 | 332 | 40 | H |
| 130 | 9 | 1 | 87 | 426 | -23.19 | -66.52 | 249 | 302 | 10 | 128 | 80 | 123 | 35 | 300 | 55 | H |
| 131 | 10 | 8 | 68 | 1453 | -23.3 | -66.5 | 221 | 253 | 24 | 87 | 65 | 77 | 20 | 241 | 68 | S1 |
| 132 | 8 | 3 | 62 | 0856 | -23.3 | -68.1 | 107 | 52 | 57 | 271 | 26 | 76 | 15 | 307 | 65 | S1 |
| 133 | 9 | 20 | 77 | 1623 | -23.35 | -68.33 | 124 | 198 | 31 | 74 | 43 | 43 | 7 | 145 | 58 | H |
| 134 | 5 | 3 | 82 | 726 | -23.47 | -68.81 | 112 | 294 | 27 | 35 | 20 | 253 | 5 | 346 | 35 | H |
| 135 | 3 | 9 | 81 | 746 | -23.57 | -66.35 | 221 | 238 | 25 | 108 | 54 | 77 | 16 | 198 | 60 | H |

TABLE 1. (continued)

| | Date mo | day | year | Time, UT | Location Latitude, deg | Longitude, deg | Depth, km | Pole 1 azimuth deg | plunge deg | Pole 2 azimuth deg | plunge deg | *T* Axis azimuth deg | plunge deg | *P* Axis azimuth deg | plunge deg | Reference |
|---|---|---|---|---|---|---|---|---|---|---|---|---|---|---|---|---|
| 136 | 5 | 10 | 86 | 200 | -23.61 | -67.70 | 171 | 285 | 5 | 19 | 43 | 70 | 25 | 322 | 33 | H |
| 137 | 6 | 7 | 78 | 1408 | -23.64 | -67.80 | 129 | 243 | 28 | 77 | 62 | 68 | 17 | 228 | 72 | H |
| 138 | 2 | 18 | 88 | 1352 | -23.68 | -67.71 | 157 | 282 | 2 | 16 | 59 | 76 | 35 | 310 | 40 | H |
| 139 | 6 | 30 | 88 | 1458 | -23.71 | -67.41 | 160 | 256 | 20 | 5 | 42 | 45 | 13 | 302 | 46 | H |
| 140 | 10 | 16 | 83 | 959 | -23.84 | -70.21 | 84 | 274 | 16 | 95 | 74 | 94 | 29 | 274 | 61 | H |
| 141 | 2 | 14 | 85 | 830 | -23.85 | -67.75 | 144 | 284 | 11 | 21 | 29 | 65 | 12 | 329 | 29 | H |
| 142 | 6 | 30 | 88 | 1521 | -23.87 | -67.05 | 192 | 241 | 8 | 129 | 69 | 77 | 34 | 220 | 50 | H |
| 143 | 9 | 3 | 82 | 2014 | -23.90 | -66.63 | 204 | 246 | 24 | 128 | 46 | 93 | 12 | 199 | 53 | H |
| 144 | 1 | 6 | 84 | 1501 | -23.92 | -68.65 | 108 | 275 | 15 | 163 | 55 | 119 | 23 | 240 | 49 | H |
| 145 | 7 | 19 | 82 | 2352 | -23.95 | -66.74 | 231 | 278 | 27 | 129 | 59 | 109 | 16 | 247 | 68 | H |
| 146 | 1 | 26 | 83 | 105 | -23.97 | -67.00 | 188 | 254 | 25 | 73 | 65 | 73 | 20 | 254 | 70 | H |
| 147 | 6 | 20 | 84 | 1956 | -23.98 | -66.97 | 187 | 236 | 9 | 125 | 67 | 74 | 33 | 213 | 49 | H |
| 148 | 6 | 23 | 85 | 655 | -24.06 | -67.10 | 197 | 245 | 8 | 115 | 77 | 74 | 36 | 233 | 52 | H |
| 159 | 8 | 19 | 87 | 752 | -24.13 | -66.89 | 182 | 271 | 28 | 81 | 62 | 88 | 17 | 284 | 73 | H |
| 150 | 3 | 12 | 86 | 2204 | -24.13 | -66.82 | 211 | 272 | 15 | 86 | 75 | 91 | 30 | 274 | 60 | H |
| 151 | 5 | 2 | 80 | 1909 | -24.13 | -66.94 | 205 | 252 | 19 | 107 | 67 | 82 | 25 | 233 | 62 | H |
| 152 | 9 | 11 | 82 | 1412 | -24.17 | -67.00 | 198 | 267 | 29 | 77 | 61 | 84 | 16 | 279 | 73 | H |
| 153 | 10 | 20 | 84 | 1759 | -24.26 | -67.06 | 209 | 284 | 25 | 130 | 63 | 113 | 19 | 262 | 68 | H |
| 154 | 11 | 22 | 79 | 0241 | -24.26 | -67.16 | 187 | 235 | 25 | 96 | 58 | 70 | 17 | 201 | 64 | C |
| 155 | 1 | 13 | 79 | 839 | -24.31 | -67.80 | 137 | 236 | 24 | 58 | 66 | 57 | 21 | 235 | 69 | H |
| 156 | 11 | 8 | 80 | 2135 | -24.34 | -67.65 | 147 | 233 | 28 | 47 | 62 | 51 | 17 | 240 | 72 | H |
| 157 | 11 | 22 | 79 | 241 | -24.34 | -67.39 | 181 | 237 | 25 | 119 | 46 | 83 | 12 | 190 | 53 | H |
| 158 | 4 | 18 | 79 | 1759 | -24.34 | -67.01 | 194 | 221 | 11 | 116 | 53 | 68 | 25 | 185 | 44 | H |
| 159 | 4 | 24 | 84 | 1827 | -24.36 | -66.95 | 178 | 215 | 6 | 119 | 45 | 69 | 25 | 178 | 35 | H |
| 160 | 8 | 12 | 84 | 1151 | -24.36 | -69.25 | 118 | 226 | 36 | 90 | 45 | 66 | 5 | 167 | 66 | H |
| 161 | 6 | 6 | 83 | 1622 | -24.38 | -66.93 | 194 | 238 | 25 | 100 | 58 | 73 | 17 | 203 | 64 | H |
| 162 | 9 | 18 | 87 | 843 | -24.41 | -69.10 | 118 | 221 | 26 | 92 | 52 | 62 | 14 | 178 | 61 | H |
| 163 | 12 | 28 | 79 | 1346 | -24.42 | -69.38 | 114 | 243 | 30 | 68 | 60 | 65 | 15 | 236 | 75 | H |
| 164 | 1 | 27 | 83 | 1901 | -24.45 | -67.17 | 191 | 242 | 14 | 126 | 59 | 83 | 26 | 210 | 52 | H |
| 165 | 6 | 11 | 70 | 0602 | -24.5 | -68.5 | 112 | 222 | 28 | 75 | 57 | 54 | 15 | 188 | 68 | S1 |
| 166 | 1 | 17 | 77 | 2127 | -24.85 | -68.67 | 134 | 296 | 41 | 93 | 46 | 2 | 78 | 105 | 3 | H |
| 167 | 6 | 17 | 71 | 2100 | -25.40 | -69.06 | 126 | 246 | 29 | 73 | 60 | 68 | 15 | 237 | 74 | C |
| 168 | 2 | 23 | 65 | 2211 | -25.7 | -70.5 | 80 | 50 | 79 | 281 | 7 | 93 | 37 | 290 | 51 | S1 |
| 169 | 10 | 31 | 87 | 511 | -25.88 | -69.80 | 66 | 345 | 11 | 248 | 30 | 204 | 12 | 301 | 29 | H |
| 170 | 11 | 17 | 81 | 711 | -25.95 | -70.08 | 69 | 222 | 10 | 54 | 79 | 220 | 55 | 44 | 35 | H |
| 171 | 8 | 3 | 78 | 1811 | -26.51 | -70.54 | 69 | 285 | 18 | 141 | 68 | 115 | 26 | 267 | 61 | H |
| 172 | 3 | 23 | 86 | 1147 | -26.70 | -70.78 | 99 | 313 | 21 | 133 | 69 | 133 | 24 | 313 | 66 | H |
| 173 | 5 | 16 | 84 | 344 | -27.17 | -67.04 | 156 | 177 | 6 | 84 | 22 | 38 | 11 | 132 | 19 | H |
| 174 | 6 | 28 | 78 | 727 | -27.54 | -70.10 | 120 | 278 | 19 | 44 | 60 | 80 | 22 | 310 | 58 | H |
| 175 | 5 | 7 | 84 | 1409 | -27.82 | -66.64 | 147 | 210 | 28 | 95 | 39 | 60 | 6 | 158 | 51 | H |
| 176 | 11 | 9 | 85 | 2213 | -27.85 | -66.64 | 165 | 211 | 25 | 82 | 53 | 51 | 16 | 170 | 60 | H |
| 177 | 8 | 18 | 84 | 410 | -27.91 | -66.81 | 182 | 213 | 32 | 70 | 52 | 48 | 10 | 167 | 69 | H |
| 178 | 2 | 25 | 87 | 1042 | -27.94 | -67.06 | 176 | 182 | 4 | 89 | 38 | 39 | 23 | 143 | 30 | H |
| 179 | 3 | 25 | 75 | 0641 | -27.95 | -66.53 | 173 | 215 | 34 | 79 | 47 | 55 | 7 | 161 | 66 | C |
| 180 | 6 | 10 | 85 | 1537 | -28.11 | -67.19 | 170 | 220 | 29 | 71 | 57 | 52 | 14 | 185 | 70 | H |
| 181 | 7 | 12 | 65 | 1357 | -28.4 | -68.3 | 118 | 50 | 50 | 235 | 39 | 52 | 5 | 258 | 84 | S1 |
| 182 | 5 | 23 | 88 | 28 | -28.48 | -68.65 | 106 | 230 | 61 | 50 | 29 | 230 | 16 | 50 | 74 | H |
| 183 | 12 | 7 | 77 | 32 | -28.57 | -67.39 | 144 | 228 | 42 | 58 | 48 | 53 | 3 | 171 | 84 | H |
| 184 | 4 | 2 | 85 | 235 | -28.77 | -68.97 | 83 | 291 | 31 | 43 | 32 | 77 | 0 | 346 | 48 | H |
| 185 | 7 | 29 | 87 | 1522 | -28.87 | -67.17 | 151 | 242 | 46 | 51 | 43 | 236 | 2 | 344 | 84 | H |
| 186 | 7 | 19 | 80 | 1152 | -29.00 | -69.68 | 129 | 216 | 64 | 22 | 25 | 206 | 20 | 9 | 70 | H |
| 187 | 5 | 5 | 88 | 1739 | -29.32 | -71.46 | 72 | 270 | 87 | 127 | 3 | 129 | 48 | 305 | 42 | H |
| 188 | 1 | 18 | 85 | 1500 | -29.41 | -70.71 | 75 | 232 | 23 | 137 | 12 | 182 | 25 | 276 | 8 | H |
| 189 | 6 | 27 | 79 | 2146 | -29.48 | -68.28 | 141 | 322 | 21 | 194 | 58 | 161 | 20 | 287 | 59 | H |
| 190 | 3 | 15 | 70 | 1239 | -29.7 | -69.5 | 119 | 243 | 64 | 77 | 25 | 252 | 19 | 89 | 69 | S1 |
| 191 | 10 | 21 | 83 | 814 | -30.64 | -69.11 | 132 | 233 | 60 | 110 | 17 | 271 | 24 | 142 | 56 | H |
| 192 | 5 | 10 | 87 | 1516 | -30.91 | -65.42 | 186 | 348 | 21 | 251 | 16 | 30 | 3 | 299 | 27 | H |
| 193 | 11 | 18 | 82 | 2039 | -31.25 | -65.86 | 166 | 245 | 22 | 39 | 66 | 57 | 22 | 263 | 66 | H |
| 194 | 10 | 24 | 85 | 148 | -31.41 | -68.64 | 124 | 333 | 46 | 173 | 42 | 344 | 2 | 244 | 80 | H |
| 195 | 11 | 8 | 84 | 1417 | -31.42 | -68.63 | 144 | 302 | 40 | 88 | 45 | 106 | 2 | 8 | 72 | H |
| 196 | 9 | 11 | 87 | 402 | -31.46 | -70.73 | 114 | 322 | 80 | 91 | 6 | 278 | 38 | 83 | 51 | H |
| 197 | 12 | 25 | 80 | 632 | -31.48 | -67.14 | 138 | 284 | 38 | 83 | 50 | 94 | 6 | 335 | 78 | H |
| 198 | 11 | 10 | 66 | 0302 | -31.9 | -68.4 | 113 | 76 | 25 | 320 | 43 | 284 | 10 | 27 | 51 | S1 |
| 199 | 9 | 6 | 82 | 1113 | -32.14 | -71.46 | 79 | 338 | 69 | 236 | 5 | 38 | 37 | 257 | 46 | H |
| 200 | 12 | 15 | 83 | 422 | -33.09 | -70.28 | 104 | 279 | 21 | 112 | 69 | 102 | 24 | 271 | 65 | H |
| 201 | 7 | 13 | 80 | 620 | -33.47 | -70.15 | 113 | 105 | 1 | 12 | 76 | 91 | 44 | 299 | 43 | H |
| 202 | 9 | 26 | 67 | 1111 | -33.6 | -70.5 | 84 | 50 | 80 | 305 | 2 | 115 | 41 | 315 | 46 | S1 |
| 203 | 5 | 9 | 84 | 2356 | -34.14 | -70.27 | 108 | 301 | 30 | 115 | 59 | 119 | 15 | 309 | 75 | H |
| 204 | 1 | 20 | 78 | 442 | -34.28 | -70.19 | 109 | 282 | 26 | 93 | 64 | 99 | 19 | 291 | 70 | H |

TABLE 1. (continued)

| | Date mo | day | year | Time, UT | Location Latitude, deg | Longitude, deg | Depth, km | Pole 1 azimuth deg | plunge deg | Pole 2 azimuth deg | plunge deg | T Axis azimuth deg | plunge deg | P Axis azimuth deg | plunge deg | Reference |
|---|---|---|---|---|---|---|---|---|---|---|---|---|---|---|---|---|
| 205 | 12 | 30 | 87 | 1156 | -35.03 | -70.81 | 112 | 297 | 3 | 36 | 69 | 99 | 38 | 318 | 45 | H |
| 206 | 8 | 3 | 80 | 300 | -35.25 | -69.99 | 164 | 272 | 70 | 89 | 20 | 87 | 65 | 270 | 25 | H |
| 207 | 4 | 6 | 81 | 1434 | -35.37 | -71.05 | 113 | 110 | 9 | 5 | 57 | 78 | 45 | 315 | 29 | H |
| 208 | 11 | 29 | 84 | 1912 | -35.50 | -71.12 | 102 | 307 | 8 | 61 | 71 | 112 | 35 | 326 | 50 | H |
| 209 | 3 | 20 | 79 | 2141 | -35.68 | -71.15 | 123 | 302 | 9 | 51 | 66 | 103 | 33 | 326 | 49 | H |
| 210 | 1 | 8 | 86 | 342 | -35.93 | -71.24 | 96 | 303 | 0 | 213 | 74 | 138 | 43 | 288 | 43 | H |
| 211 | 12 | 26 | 79 | 1943 | -36.00 | -71.34 | 111 | 265 | 5 | 109 | 84 | 87 | 40 | 262 | 50 | H |
| 212 | 2 | 9 | 86 | 2332 | -36.13 | -71.27 | 125 | 284 | 76 | 102 | 14 | 101 | 59 | 282 | 31 | H |
| 213 | 12 | 15 | 81 | 1231 | -36.28 | -71.36 | 105 | 218 | 9 | 67 | 80 | 42 | 36 | 212 | 54 | H |
| 214 | 9 | 5 | 86 | 606 | -37.05 | -71.76 | 81 | 135 | 2 | 39 | 66 | 111 | 42 | 336 | 38 | H |
| 215 | 1 | 2 | 78 | 827 | -38.14 | -71.10 | 144 | 99 | 7 | 3 | 37 | 315 | 20 | 58 | 31 | H |

Focal mechanism parameters for each event are listed with the azimuth and plunge for poles of both nodal planes, the *P* and *T* axes given. References are as follows: S1, *Stauder* [1973]; S2, *Stauder* [1975]; H, *Dziewonski et al.* [1983a, 1983b, 1984a, 1984b, 1984c, 1985a, 1985b, 1985c, 1985d, 1985e, 1986a, 1986b, 1987a, 1987b, 1987c, 1987d, 1988a, 1988b, 1988c, 1989a, 1989b, 1989c; and C, this study.

TABLE 2. Focal Mechanism Solutions of Deep Earthquakes Beneath the Central Andes

| | Date mo | day | year | Time, UT | Location Latitude, deg | Longitude, deg | Depth, km | Pole 1 azimuth deg | plunge deg | Pole 2 azimuth deg | plunge deg | T Axis azimuth deg | plunge deg | P Axis azimuth deg | plunge deg | Reference |
|---|---|---|---|---|---|---|---|---|---|---|---|---|---|---|---|---|
| 1 | 1 | 17 | 84 | 332 | -8.90 | -71.35 | 619 | 281 | 67 | 96 | 23 | 277 | 22 | 92 | 68 | H |
| 2 | 5 | 1 | 85 | 1327 | -9.17 | -71.26 | 616 | 259 | 61 | 82 | 29 | 261 | 16 | 85 | 74 | H |
| 3 | 5 | 3 | 85 | 1528 | -9.22 | -71.25 | 606 | 220 | 56 | 65 | 31 | 235 | 13 | 99 | 72 | H |
| 4 | 12 | 24 | 84 | 1336 | -9.53 | -71.42 | 556 | 242 | 30 | 93 | 56 | 74 | 14 | 206 | 70 | H |
| 5 | 6 | 2 | 83 | 2012 | -9.58 | -71.24 | 614 | 258 | 52 | 93 | 37 | 266 | 7 | 134 | 79 | H |
| 6 | 1 | 12 | 72 | 0959 | -6.9 | -71.8 | 580 | 70 | 28 | 275 | 60 | 259 | 16 | 43 | 70 | S2 |
| 7 | 11 | 9 | 63 | 2115 | -9.0 | -71.5 | 600 | 80 | 44 | 262 | 46 | 261 | 1 | 180 | 89 | S2 |
| 8 | 2 | 15 | 67 | 1611 | -9.0 | -71.3 | 597 | 77 | 35 | 257 | 55 | 257 | 10 | 77 | 80 | S2 |
| 9 | 11 | 3 | 65 | 0139 | -9.1 | -71.3 | 593 | 105 | 50 | 89 | 39 | 263 | 5 | 136 | 81 | S2 |
| 10 | 11 | 10 | 63 | 0100 | -9.2 | -71.5 | 600 | 87 | 46 | 275 | 44 | 91 | 1 | 339 | 86 | S2 |
| 11 | 4 | 9 | 77 | 404 | -10.02 | -71.18 | 575 | 259 | 43 | 90 | 47 | 84 | 2 | 192 | 84 | H |
| 12 | 8 | 15 | 63 | 1725 | -13.8 | -69.3 | 543 | 98 | 37 | 322 | 44 | 299 | 4 | 37 | 66 | S2 |
| 13 | 6 | 15 | 87 | 2105 | -19.10 | -63.87 | 606 | 304 | 67 | 42 | 3 | 242 | 38 | 19 | 44 | H |
| 14 | 8 | 14 | 87 | 2220 | -19.12 | -63.94 | 590 | 304 | 79 | 59 | 5 | 248 | 39 | 47 | 49 | H |
| 15 | 8 | 23 | 68 | 2236 | -22.0 | -63.5 | 537 | 261 | 35 | 100 | 53 | 89 | 9 | 223 | 76 | S1 |
| 16 | 11 | 29 | 85 | 402 | -22.76 | -63.62 | 551 | 353 | 62 | 99 | 9 | 301 | 31 | 72 | 47 | H |
| 17 | 11 | 6 | 87 | 1847 | -22.84 | -63.63 | 541 | 318 | 84 | 78 | 3 | 263 | 42 | 73 | 48 | H |
| 18 | 12 | 20 | 80 | 2026 | -24.37 | -63.42 | 574 | 293 | 71 | 80 | 16 | 268 | 29 | 65 | 59 | H |
| 19 | 2 | 4 | 77 | 746 | -24.69 | -63.36 | 565 | 311 | 83 | 63 | 3 | 249 | 42 | 56 | 47 | H |
| 20 | 12 | 8 | 62 | 2127 | -25.8 | -63.4 | 620 | 75 | 5 | 336 | 60 | 279 | 33 | 47 | 42 | S1 |
| 21 | 12 | 20 | 66 | 1226 | -26.1 | -63.2 | 589 | 60 | 15 | 290 | 67 | 253 | 28 | 37 | 56 | S1 |
| 22 | 3 | 5 | 65 | 1432 | -27.0 | -63.3 | 573 | 75 | 20 | 305 | 60 | 271 | 21 | 43 | 59 | S1 |
| 23 | 9 | 29 | 62 | 1517 | -27.1 | -63.5 | 577 | 70 | 10 | 320 | 62 | 270 | 30 | 42 | 48 | S1 |
| 24 | 1 | 10 | 83 | 1232 | -27.30 | -63.39 | 565 | 253 | 58 | 52 | 30 | 240 | 15 | 26 | 73 | H |
| 25 | 4 | 1 | 81 | 1803 | -27.31 | -63.32 | 561 | 235 | 67 | 72 | 22 | 247 | 23 | 82 | 66 | H |
| 26 | 1 | 17 | 67 | 0107 | -27.4 | -63.3 | 590 | 74 | 18 | 300 | 64 | 267 | 24 | 49 | 59 | S1 |
| 27 | 12 | 9 | 64 | 1335 | -27.5 | -63.2 | 586 | 75 | 15 | 323 | 54 | 279 | 23 | 39 | 49 | S1 |
| 28 | 9 | 5 | 79 | 1356 | -27.55 | -63.27 | 566 | 287 | 59 | 67 | 24 | 261 | 19 | 35 | 64 | H |
| 29 | 9 | 9 | 67 | 1006 | -27.7 | -63.1 | 578 | 78 | 25 | 273 | 64 | 262 | 19 | 65 | 69 | S1 |
| 30 | 10 | 22 | 77 | 1757 | -27.95 | -62.97 | 615 | 245 | 2 | 116 | 86 | 242 | 47 | 68 | 43 | H |
| 31 | 11 | 17 | 83 | 1039 | -28.20 | -63.22 | 574 | 258 | 59 | 73 | 31 | 255 | 14 | 67 | 76 | H |
| 32 | 12 | 21 | 83 | 1205 | -28.23 | -63.20 | 600 | 267 | 13 | 112 | 76 | 259 | 57 | 92 | 32 | H |
| 33 | 12 | 29 | 86 | 1253 | -28.28 | -63.03 | 626 | 260 | 6 | 28 | 81 | 268 | 50 | 74 | 39 | H |
| 34 | 12 | 22 | 83 | 1153 | -28.33 | -63.04 | 600 | 276 | 6 | 170 | 69 | 255 | 48 | 114 | 36 | H |
| 35 | 10 | 27 | 87 | 2158 | -28.73 | -62.96 | 604 | 274 | 82 | 101 | 8 | 280 | 37 | 102 | 53 | H |
| 36 | 10 | 31 | 85 | 2149 | -28.75 | -63.19 | 596 | 305 | 52 | 55 | 15 | 261 | 22 | 18 | 48 | H |

Focal mechanism parameters for each event are listed with the azimuth and plunge for poles of both nodal planes, the *P* and *T* axes given. References are as follows: S1, *Stauder* [1973]; S2, *Stauder* [1975]; H, *Dziewonski et al.* [1983a, 1983b, 1984a, 1984b, 1984c, 1985a, 1985b, 1985c, 1985d, 1985e, 1986a, 1986b, 1987a, 1987b, 1987c, 1987d, 1988a, 1988b, 1988c, 1989a, 1989b, 1989c; and C, this study.

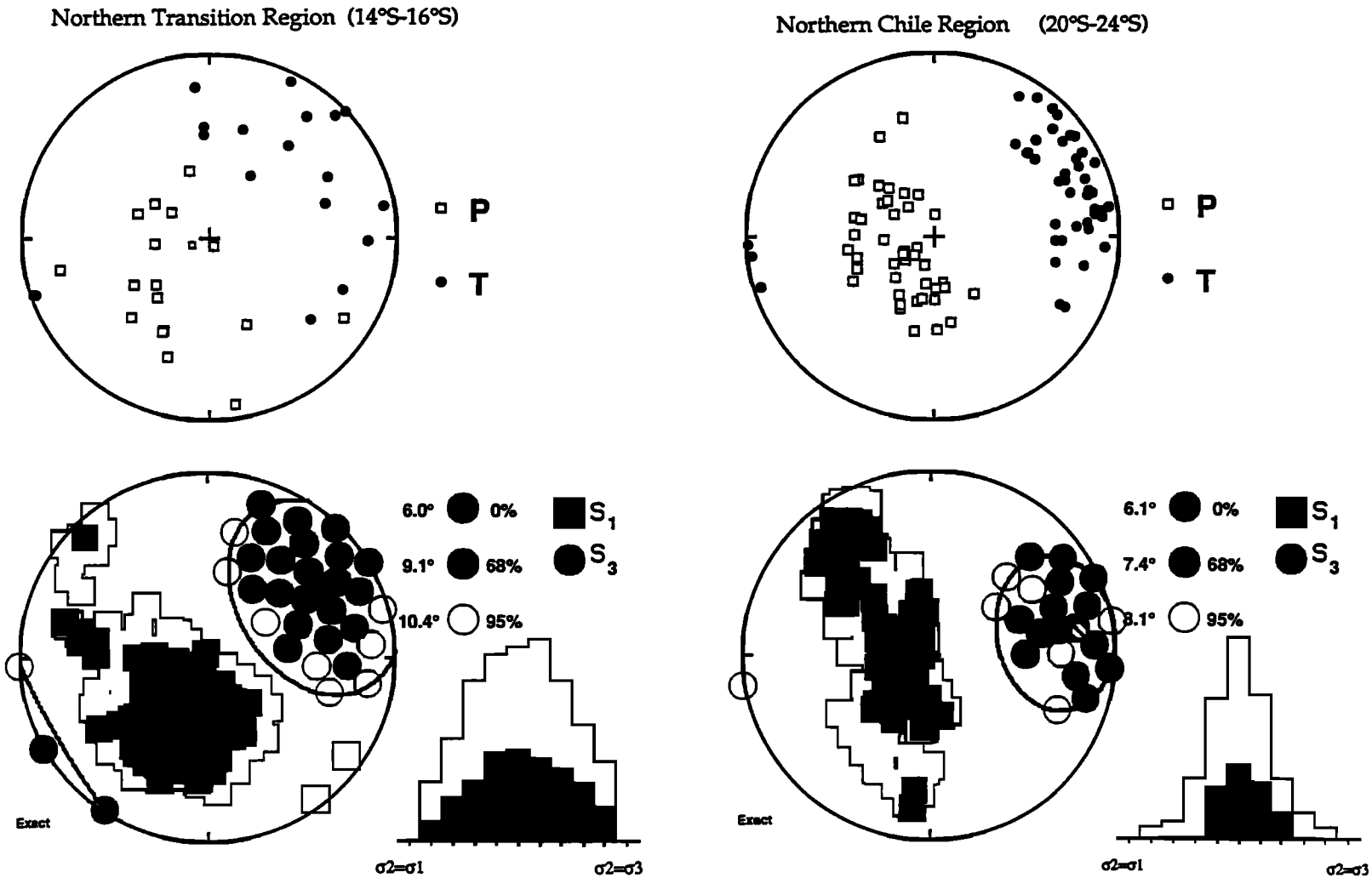


(a) Northern Transition Region; The best fitting stress model has σ1: strike=209° and dip=59°; σ2: strike=314° and dip=9°; σ3: strike=50° and dip=30°. The downdip direction in the region varies in strike from 45°-105° and in dip angle from 12° to 34°.

(b) Northern Chile Region; The best fitting stress model has σ1: strike=278° and dip=76°; σ2: strike=164° and dip=6°; σ3: strike=73° and dip=12°. The regional downdip direction is: strike=80° and dip=18°.

Fig. 13. Results from an inversion method for orientation of principal stress axes are shown. The upper plot in each figure is an equal-area projection of *P* and *T* axes for focal mechanisms within the specified geographic region. The lower plots show equal-area projections of the σ1 and σ3 directions that require the least rotation to align the slip directions observed in the focal mechanisms with that predicted by the stress model. The average rotational misfit for each confidence limit is shown at the upper right; the histograms at the lower right show the magnitude of σ2 relative to σ1 and σ3. The striped areas show the projection of the regional downdip direction onto the stereonet.

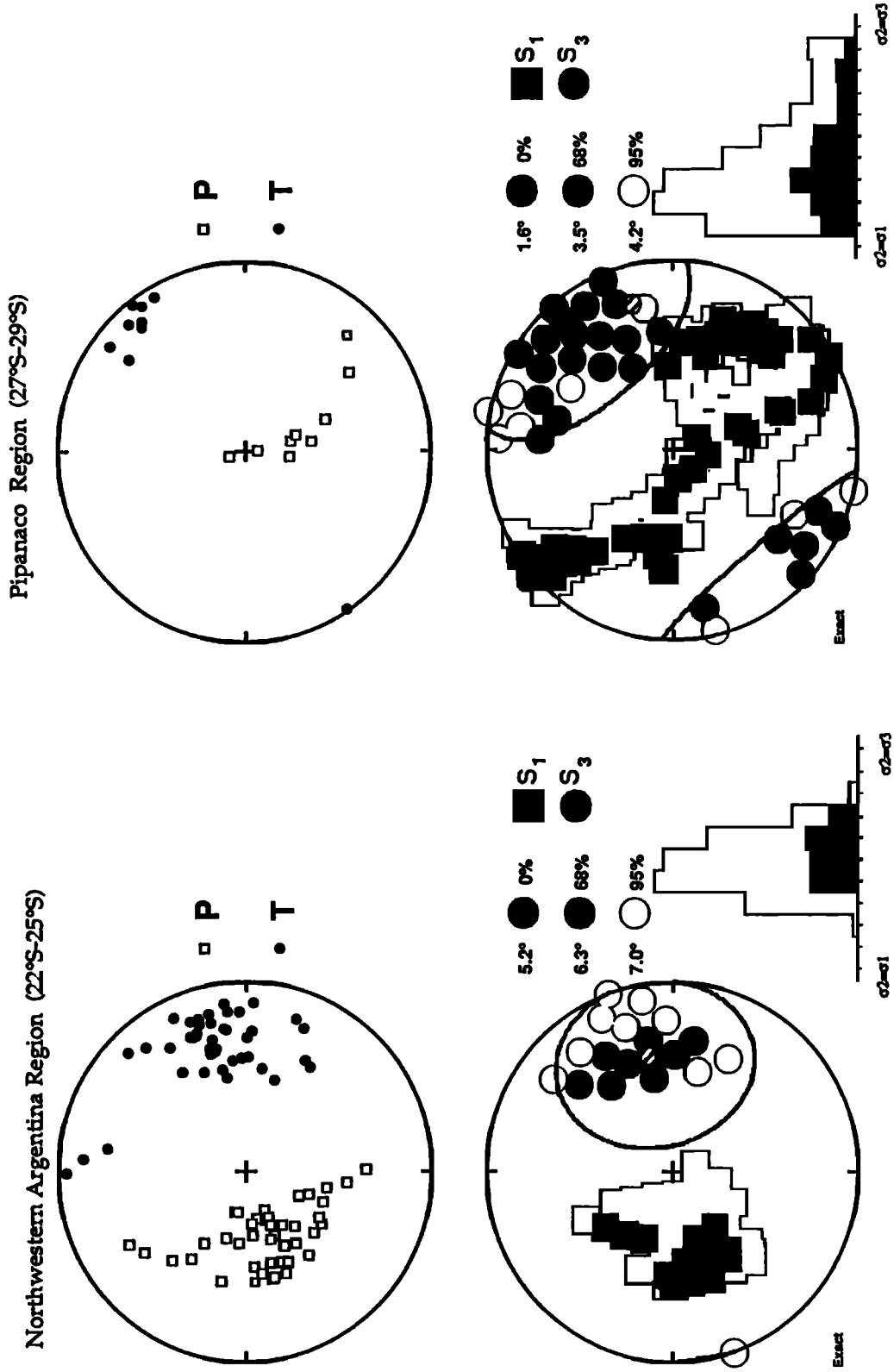


(c) Northwestern Argentina Region; The best fitting stress model has σ1: strike=260° and dip=51°; σ2: strike=163° and dip=6°; σ3: strike=68° and dip=38°. The regional downdip direction is: strike=80° and dip=34°.

(d) Pipanaco Region; The best fitting stress model has σ1: strike=319° and dip=11°; σ2: strike=154° and dip=78°; σ3: strike=50° and dip=3°. The regional downdip direction is: strike=75° and dip=22°.

Fig. 13. (continued)

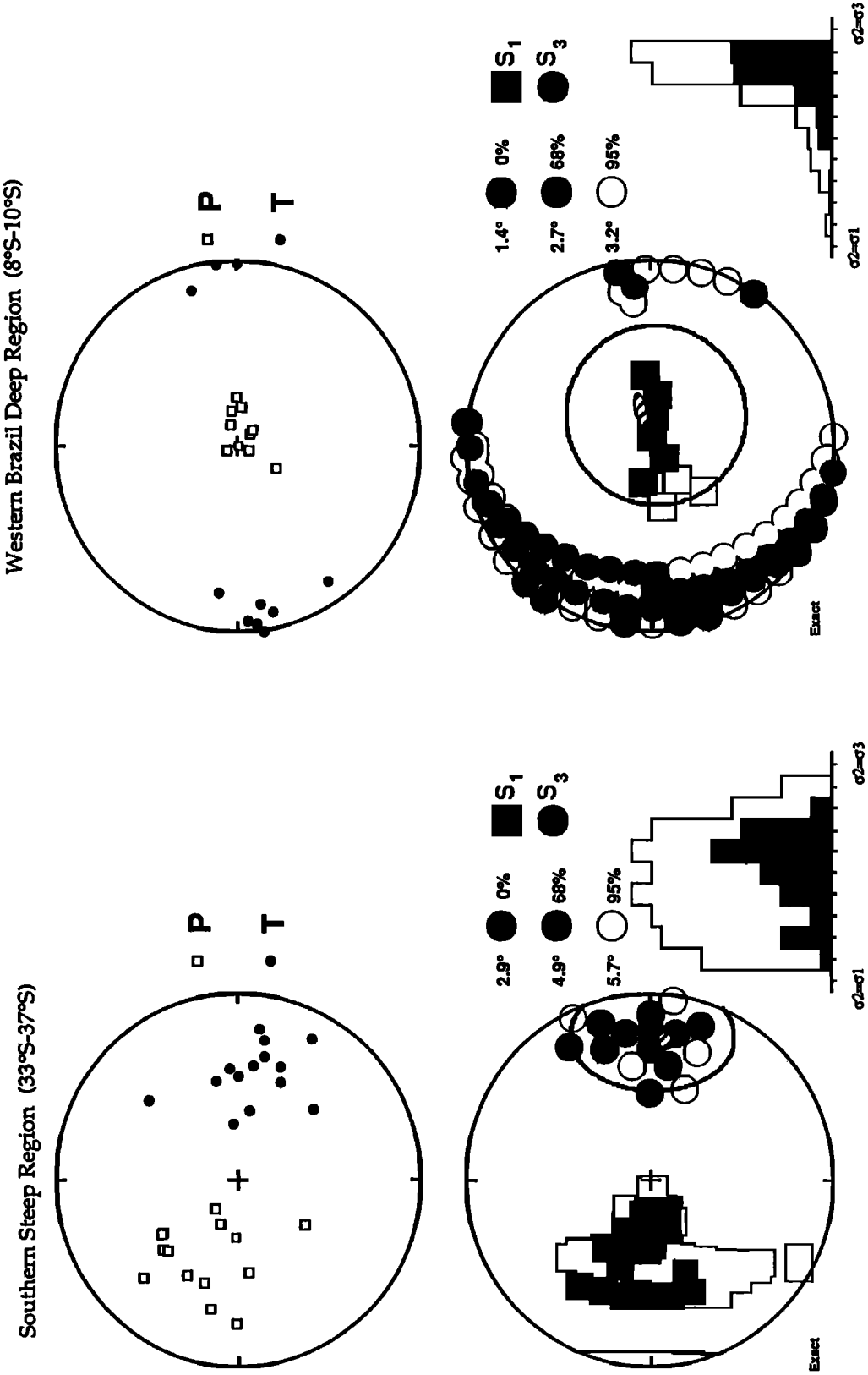


(e) Southern Steep Region; The best fitting stress model has σ1: strike=272° and dip=69°; σ2:strike=181° and dip=0°; σ3: strike=91° and dip=21°. The regional downdip direction is: strike=95° and dip=24°.

(f) Western Brazil Deep Region; The best fitting stress model has σ1: strike=100° and dip=67°; σ2: strike=307° and dip=21°; σ3: strike=213° and dip=9°. The regional downdip direction is: strike=70° and dip=70-80°.

Fig. 13. (continued)

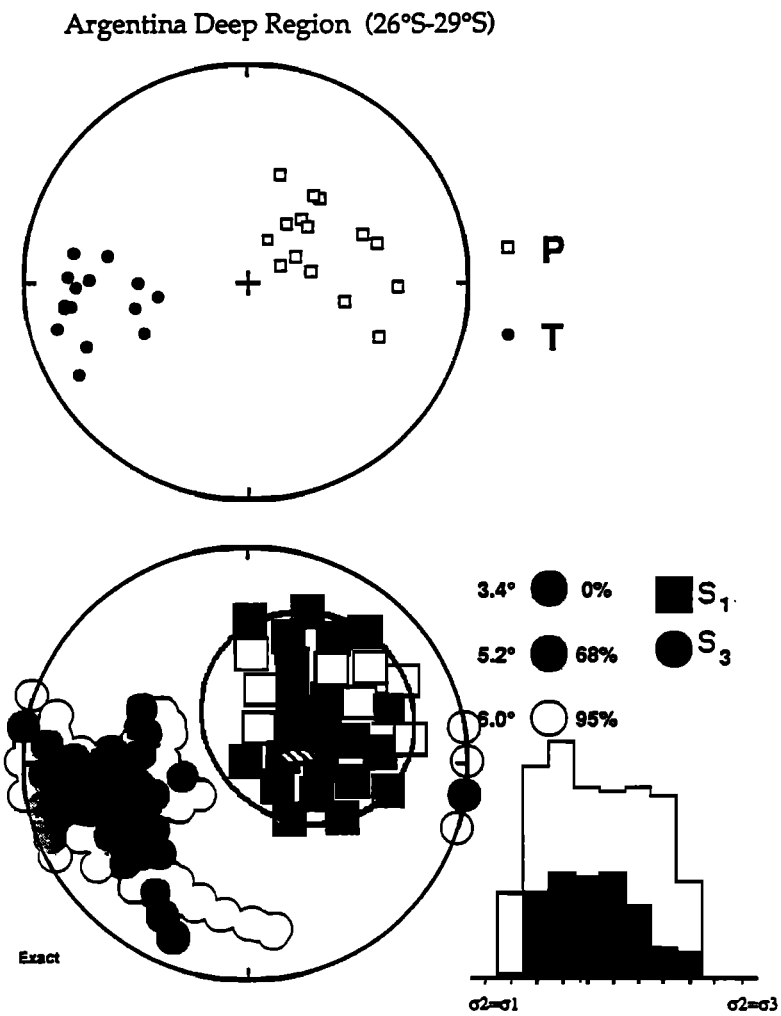


(g) Argentina Deep Region; The best fitting stress model has σ1:strike=52° and dip=60°; σ2: strike=165° and dip=13°; σ3: strike=262° and dip=27°. The regional downdip direction is: strike=80° and dip=60-80°.

Fig. 13 (continued)

*Pipanaco Region (27°S to 29°S)*

Focal mechanisms exist for only nine earthquakes in the WBZ beneath the Pipanaco Basin, NW Argentina. *T* axes for these events are very tightly clustered and with a northeasterly strike and shallow plunge; the *P* axes are not as consistent. The relative orientations of σ3 and the regional downdip direction are seen in Figure 13d; the best fitting stress model for this area has σ3 where strike=060° and dip=19°E. Although the range of possible solutions is not as tight as for the southern "steep" region, the best fitting σ3 lies close to the downdip direction.

*Southern "Steep" Region (33°S to 37°S)*

Focal mechanism solutions exist for 14 intermediate-depth events in the region of moderate eastward dip beneath central Chile. Both the *P* and *T* axes for these events are distributed within fairly tight zones, with the center of the *T* axis cluster closely approximating the downdip direction in the region (Figure 13e). The best fitting stress model for this portion of the WBZ has σ3 where strike=091° and dip=21°E. In the southern "steep" region, σ3 is more closely aligned with the downdip direction than is the center of the *T* axis cluster.

*Deep Earthquakes*

The 28 deep events (h>350 km) for which focal mechanism solutions exist were separated into two groups, one beneath western Brazil (8°S to 10°S), the other beneath western Argentina (26°S to 29°S). The stereo projections corresponding to deep earthquakes in Figures 13f and 13g show P axes in both regions trending to the east and plunging steeply; *P* axes for events beneath western Brazil are more tightly clustered and have a consistently steeper plunge than those beneath western Argentina.

The seismically active portions of the deep slab are separated from the shallower portions of the WBZ by a prominent gap in slab seismicity (Figure 2), a gap that persists 325 km updip from the western Argentina zone of deep earthquakes and 450 km updip from the western Brazil zone. The presence of this gap and the narrowness of the deep seismic zones make it difficult to determine accurately a downdip direction in the vicinity of the deep events. Minimum eastward dips of 60° in western Argentina and 70° in western Brazil can be estimated by assuming the slab to be continuous across the seismic gap; a maximum dip for both segments of 80° is estimated from the slight increase in focal depths observed across the narrow zones.

The results of the inversion give a best fitting σ1 where strike= 100° and dip=67° E-NE for the northern zone of deep earthquakes and a best fitting σ1 where strike= 52° and dip=60°E for the southern zone. The distribution of *P* axes and the results of the stress inversion are consistent with the observation that the zone of deep earthquakes is much closer to shallower contours in western Brazil than in western Argentina and the reasonable inference that the slab is steeper in this region.

The inversion results from each grouping of events support earlier conclusions that the WBZ seismicity is a response to downdip stresses in the descending slab, with σ3 dominating above 350 km and σ1 dominating at greater depths [ *Isacks and Molnar,* 1971; *Stauder* 1973,1975; *Apperson and Frohlich,* 1987; *Schneider and Sacks,* 1987]. Although the orientations of σ1 and σ2 for intermediate-depth events in the descending slab are not as consistent as those observed for σ3, some generalizations can be made. The axis of maximum compression (σ1) is typically perpendicular to the slab; σ2 is typically along strike of the slab, nearly horizontal, and roughly equidistant in magnitude between σ1 and σ3. The orientations of σ1 and σ2 can be interpreted as simply reflecting the difference in lateral continuity of the slab; that is, the minimum extensive stress for a thin, infinite plate under tension is expected, and in this case is observed to occur normal to the plane of the slab.

The only exception to the consistency of the σ1 and σ2 directions occurs in the Pipanaco cluster, immediately south of the large aseismic gap between 25°S and 27°S. The solutions for this region show σ1 to be horizontal, along strike, and not very different in magnitude than σ2. If, as has been proposed by *Febrer et al.* [1982], the slab in this region is completely separated from the rest of the descending plate, we might expect such a drop in along strike confining stresses. We hasten to qualify this observation with the reminder that the data set for this region is very small, and the range of possible solutions is correspondingly large.

## DISCUSSION

This new compilation of teleseismic data lends support to earlier conclusions about the along strike variability in dip angle of the subducted Nazca plate and adds to many recent studies defining the geometrical nature of the transitions in slab dip. The more detailed image of the shape of the subducted slab permits more precise statements about the spatial relationship between slab geometry and deformation within the overriding continental plate. *Isacks* [1988] suggests that these relationships explain how slab dip affects the style and extent of deformation in the overriding plate and determine the shape of the plate margin. Two important questions, however, remain unanswered; Why does the slab geometry change from flat to steep, and why do the transitions in dip occur where they do?

In one hypothesis a causal relation is suggested between the subduction of submarine bathymetric highs on the Nazca plate and low angle subduction. A spatial association has been

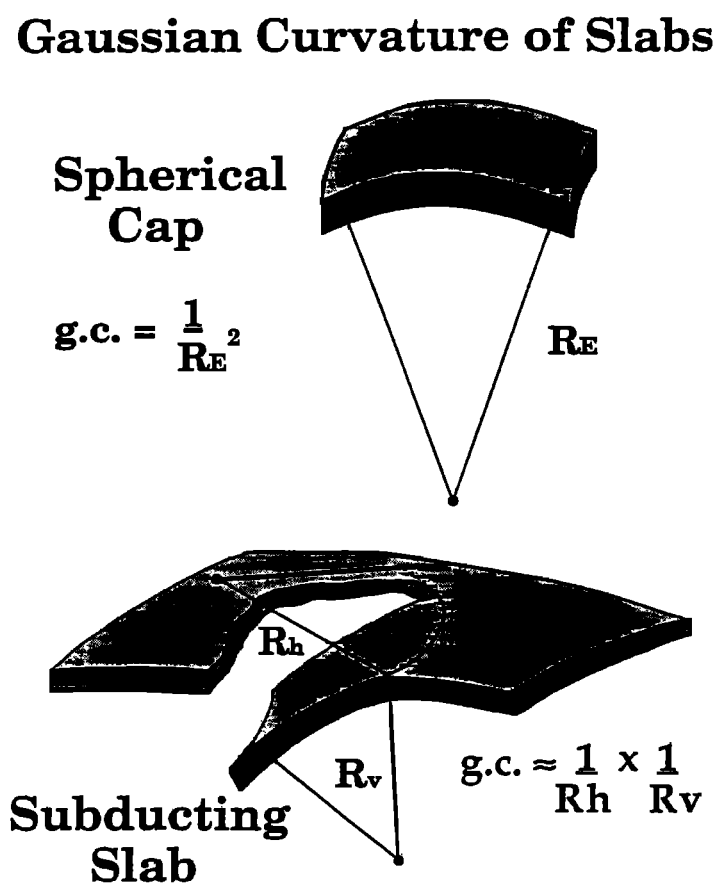


Fig. 14. Gaussian curvature of a surface is defined as the product of the minimum and maximum radii of curvature. A spherical cap, representing presubduction oceanic lithosphere, has identical positive radii of curvature and thus positive Gaussian curvature. The subducting slab (bottom) has both positive vertical curvature (convex-up slab) and positive lateral curvature (concave-seaward trench). However, typical subduction zones have positive vertical curvature but negative lateral curvature (convex-seaward trench) and thus a negative Gaussian curvature.

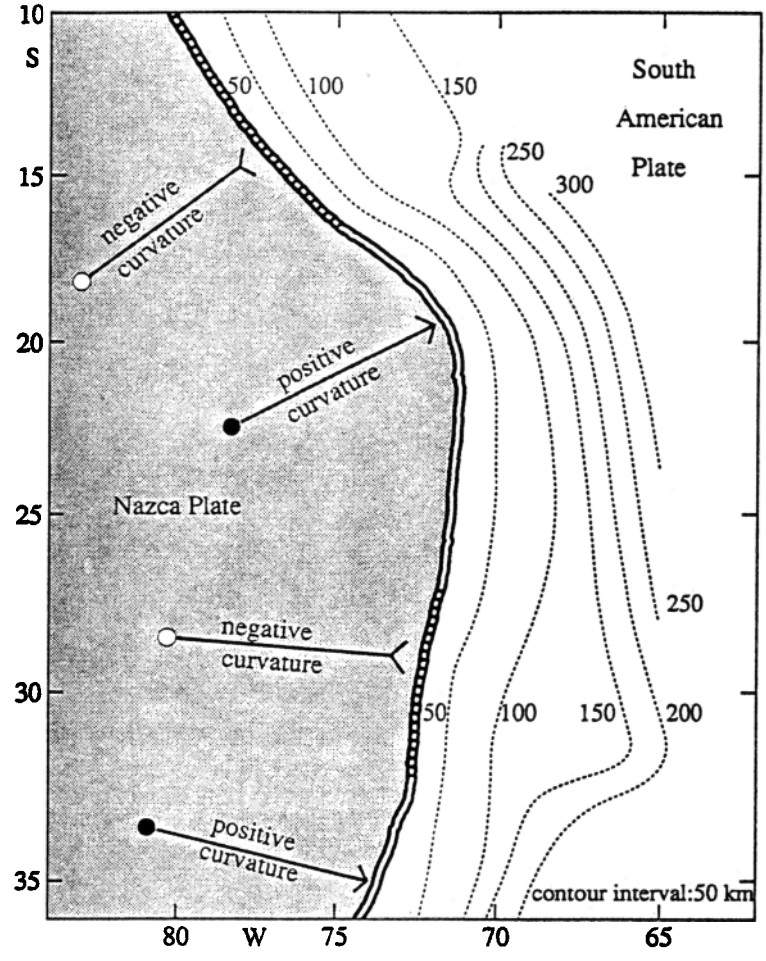


Fig. 15. Curvature of the South America-Nazca plate boundary. Convex-seaward segments of the plate margin are defined as having negative radii of curvature; concave-seaward segments have positive radii. WBZ depth contours (dashed lines) show that the regions of flat subduction (10°S to 15°S,28°S to 33°S), which have a concave-up form, are associated with convex-seaward segments of the plate margin. Regions of steeper subduction (15°S to 28°S,33°S to 36°S), which have a convex-up form, are associated with concave-seaward segments of the margin. Both combinations result in a positive Gaussian curvature, consistent in sign with the original curvature of the oceanic lithosphere.

noted between subduction of the Nazca Ridge and the low angle WBZ beneath central Peru [*Vogt et al.*, 1976; *Pilger*, 1981; *Cross and Pilger*, 1982] and subduction of the Juan Fernandez seamounts west of the zone of subhorizontal WBZ beneath central Chile/western Argentina [*Barazangi and Isacks*, 1976; *Smalley and Isacks*, 1987]. The evidence for this argument is not completely convincing. Although on a regional scale the projection of the ridge beneath southern Peru appears coincident with the narrowing of the northern Altiplano, a closer examination shows the warping of WBZ contours, extinction of the volcanic arc, and limit of the high, undissected plateau all occur 150-200 km south of the projected position of the subducting ridge (Figure 2*a*). The case for bathymetrically influenced flattening near 32°S is no more compelling, as the flattening begins at least 700 km to the north of the intersection of the Juan Fernandez seamounts with the Chile trench. The Perdida ridge (Figure 2*a*), a more substantial bathymetric feature than the Juan Fernandez seamounts, meanwhile, is being subducted updip from the most steeply dipping portion of the central Andean WBZ, without any obvious deforming impact on the shape of the subducted slab. A final problem exists reconciling arguments for the presumed anomalous buoyancy of the subducted ridge with the expected transformation of excess oceanic crust to high-density eclogite at about 80 km depth, above the zone of flattening [*Kelleher and McCann*, 1976].

To attribute the flattening to subduction of younger oceanic lithosphere is also unsatisfactory. Whereas the oceanic lithosphere subducted north of the Nazca Ridge is younger (~40 Ma) than that immediately to the south (~46 Ma) [*Handschumacher*,1976], beneath central Chile the opposite relation is seen: An equivalent or greater decrease in the age of subducted lithosphere, from 50 Ma to 40 Ma [*Lowrie and Hey*, 1981], corresponds to the southward steepening of subduction angle.

*Bevis and Isacks* [1984] suggested that the flattening of the subducted plate beneath southern Peru is a geometric accommodation to the arcuate shape of the leading edge of the South American plate in that region. The western margin of South America presents a variety of shapes to the approaching Nazca plate, from convex-seaward (8°S to 15°S) to concave-seaward (15°S to 24°S), then, repeating the sequence to the south with much less curvature, convex-seaward (24°S to 32°S), and concave-seaward (32°S to 36°S). The correlation between changes in plate margin curvature and transitions in slab dip may reflect the important role played by the South

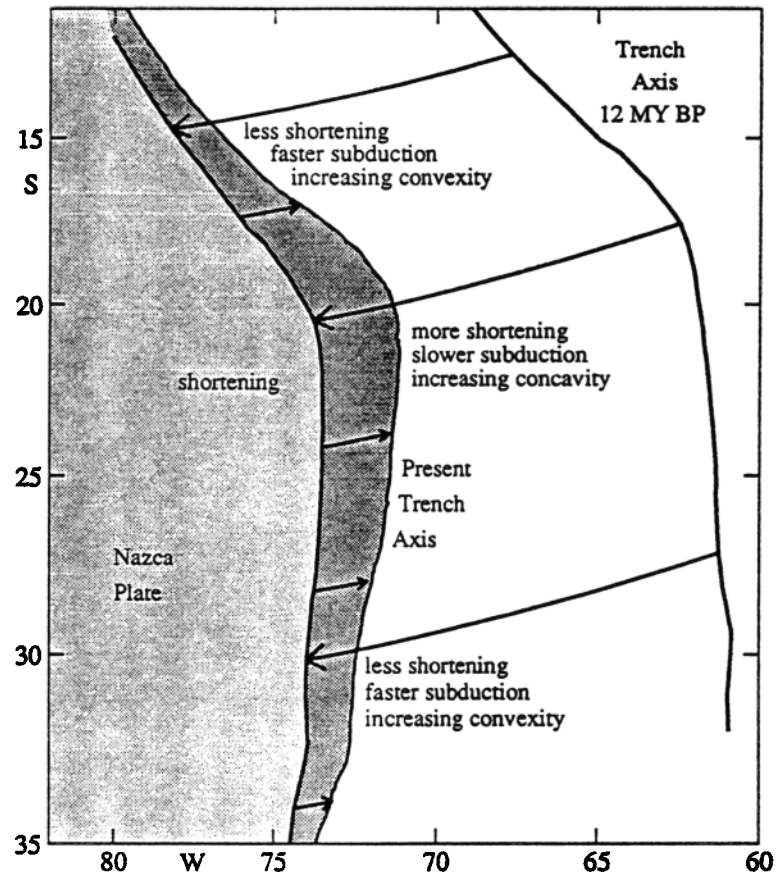


Fig. 16. The hypothesized migration and evolution of the South America-Nazca plate margin [after *Isacks*, 1988]. Here the Nazca plate is held fixed while the South American plate is rotated from its hypothetical position 12 Ma before present. The darkly shaded area shows the variation in along-strike shortening that results in the transformation of the old, broadly concave-seaward trench to the more complex modern form. The plate margin in regions of lesser shortening (faster subduction) has become convex-seaward; in regions of greater shortening (slower subduction) the margin has become increasingly concave-seaward.

American plate in determining subduction angle, not only in southern Peru, but all along the central Andean subduction zone.

To demonstrate how the continental plate governs the subduction dip angle, we return to *Bevis'* [1986] discussion of Gaussian curvature. *Bevis* [1986] pointed out that an inherent trait of inextensible surfaces is constant Gaussian curvature, defined as the product of the reciprocals of the minimum and maximum radii of curvature (Figure 14). By convention, a convex-up surface has a positive radius of curvature, a concave-up surface has negative curvature; on a globe, concave-seaward arcs have positive radii of curvature, while convex-seaward arcs have negative radii.

*Bevis* [1986] explained that a perfectly inextensible spherical cap, representing presubduction oceanic lithosphere, cannot assume the shape observed in most WBZs. A spherical cap has positive, identical radii of curvature and thus a positive Gaussian curvature; subduction margins, however, typically have a convex-seaward, convex-up form and thus a negative Gaussian curvature. Following this reasoning, we should not, in general, expect subducting slabs to behave as perfectly inextensible surfaces.

Nowhere along the convergent margin of South America do the values of total Gaussian curvature approach those of a spherical cap with radius 6355 km, that of unsubducted oceanic lithosphere. Vertical radii of curvature for the WBZ never exceed 1000 km and the radius of curvature of the plate margin ranges only from 500 to 2000 km. Thus the subducted slab is certainly not perfectly inextensible near the zone of interplate contact. Indeed, focal mechanisms of shallow earthquakes (h<70 km) within the oceanic lithosphere near the plate margin show that the slab is pervasively fractured and strained by bending stresses imposed during subduction [*Kadinsky-Cade*, 1985; *Isacks and Barazangi*, 1977]. However, the focal mechanisms of deeper slab events show a region-wide pattern of downdip T axes, from which we infer that a surface exists within the slab that remains capable of transmitting stresses [*Schneider and Sacks*, 1987; *Stauder*, 1973, 1975; *Apperson and Frohlich*, 1987] (see also this study].

We postulate that the ability to transmit stresses allows the slab to assume a shape consistent with the original positive Gaussian curvature: The descending plate responds to the changing polarity of lateral curvature in the South American margin by reversing the orientation of its vertical curvature (Figure 15). When the plate boundary is concave-seaward (positive curvature) as between 16°S and 24°S and south of 33°S, the slab descends with a convex-up geometry (positive curvature). North of 15°S and between 28°S and 33°S, the plate boundary is convex-seaward (negative curvature), and the slab assumes a concave-up shape (negative curvature) below

the zone of interplate contact. The flexure into a concave-up form below the interplate contact zone results in the flattened portions of the slab observed to the east. Farther east still, downdip of the low-angle subduction, the slab resumes its convex-up (positive curvature) descent into the mantle. The contours of the subducted slab at depths of 125 km and deeper in these regions (12° to 15°S and 28° to 32°S) indicate that the slab is again bent laterally into a concave-seaward (positive curvature) form.

*Isacks* [1988] proposed that the present shape the plate margin may be due to the variable shortening rate along the plate margin. Between 15°S and 27°S, the region of magmatic activity and a wide plateau, the continental plate appears to have undergone considerably more shortening than the regions overlying the horizontally subducting slabs to the north and south. Whatever the cause for the variation in total shortening, the accompanying effect has been a variation in the subduction rate along the margin. The convergence rate between the Nazca and South American plates is roughly constant along a great length of their shared plate margin (the pole of rotation being 70° to 85° distant). As the total convergence is the sum of subduction and intraplate deformation, along-strike variations in shortening of the continental plate are matched by compensating variations in subduction. In regions of lesser shortening, found above the horizontally subducting slab, more of the convergence between the plates is taken up through subduction, resulting in an increase in the convexity of the margin (Figure 16).

If the model of *Isacks* [1988] is correct and the presence of an asthenospheric wedge above the steeply dipping slab contributes to an increased amount crustal shortening, a positive feedback relationship may exist between plate margin shape and slab dip. The increase in seaward convexity of the trench axis to the north and south of the region of greater shortening results in a decrease in slab dip in these regions. The decrease in slab dip, by squeezing out the asthenospheric material between the subducting slab and overriding continent, results in less heat transfer and still lower shortening rates. Lower shortening rates, in turn, lead to a further increase in convexity.

## CONCLUSIONS

Nine years of teleseismic locations have been added to the most recent continental-scale study of the South American WBZ, providing significant detail to the knowledge of the shape of the subducted plate beneath the central Andes. The new data support previous resolutions of a sharply flexed plate with southward transitions from flat to 30°-dipping geometries beneath southern Peru (near 15°S) and central Chile (near 33°S). In contrast, the southward transition from 30° slab dip beneath Bolivia to a nearly horizontal dip in the region of 28°S to 32°S appears to be gradual. Contours of hypocentral depth and detailed cross sections of seismicity and topography and volcanic centers were used to detail the relationships between slab geometry and upper plate tectonics. The transitions from a wide, volcanically active plateau to narrow, nonvolcanic cordillera near 15°S and near 27°S to 28°S are associated with changes in curvature of the subducted slab, from convex upward to concave upward, just downdip from the Nazca-South America plate boundary interface. An inversion for the orientation and relative magnitudes of the principal stresses in the subducted slab using focal mechanisms agrees with all previous studies of stress orientation in the descending plate, with downdip extensional stress dominating above 350 km and downdip compression dominating at greater depths.

*Acknowledgments.* - We thank John Gephart for help with manipulation and interpretation of focal mechanism data and for a fresh perspective on Andean tectonics. Muawia Barazangi was available for many valuable discussions and critical analyses of our work. Careful, thoughtful reviews provided by Michael Bevis and Thomas Boyd resulted in an improved manuscript. This study was supported by NSF grants EAR-8804976 and EAR-9005222.

## REFERENCES

Allmendinger, R. W., V. A. Ramos, T. E. Jordan, M. Palma, and B. L. Isacks, Paleogeography and Andean structural geometry, northwest Argentina, *Tectonics, 2*, 1-16, 1983.

Allmendinger, R. W., D. Figueroa, D. Snyder, C. Mpodozis, J. Beer, and V. Ramos, Foreland shortening and crustal balancing in an amagmatic orogen: The Andes at 30°S latitude, *Tectonics, 9*, 789-809, 1990.

Apperson, K. D., and C. Frohlich, The relationship between Wadati-Benioff zone geometry and P, *T*, and *B* axes of intermediate and deep focus earthquakes, *J. Geophys. Res., 92*, 13,821-13,831, 1987

Barazangi, M., and B. L. Isacks, Spatial distribution of earthquakes and subduction of the Nazca Plate beneath South America, *Geology, 4*, 686-692, 1976.

Barazangi, M., and B.L. Isacks, Subduction of the Nazca plate beneath Peru: Evidence from spatial distribution of earthquakes, *Geophys. J. R. Astron. Soc., 57*, 537-555, 1979.

Bevis, M., The curvature of Wadati-Benioff zones and the torsional rigidity of subducting plates, *Nature, 323*, 52-53, 1986.

Bevis, M., and B.L. Isacks, Hypocentral trend surface analysis: Probing the geometry of Benioff Zones, *J. Geophys. Res., 89*, 6153-6170, 1984.

Boyd, T. M., J. A. Snoke, I. S. Sacks and A.B. Rodriguez, High resolution determination of the Benioff zone geometry beneath southern Peru, *Bull. Seismol. Soc. Am., 74*, 559-568, 1984.

Cahill, T. and B. L. Isacks, An apparent double-planed Benioff zone beneath northern Chile resulting from misidentification of reflected phases, *Geophys. Res. Lett., 13*, 333-336, 1986.

Chinn, D., B. L. Isacks, and M. Barazangi, High frequency shear wave propagation along the western margin of South America: Implications for oceanic Sn and the Altiplano, *Geophys. J. R. Astron. Soc, 60*, 209, 1980.

Creager, K.C., and T.M. Boyd, The geometry of Aleutian subduction: Three-dimensional flow model, *J. Geophys. Res., 96*, 2293-2307, 1991.

Cross, T. A., and R. H. Pilger, Jr., Control of subduction geometry, location of magmatic arcs, and tectonics of arc and back-arc regions, *Geol. Soc. Am. Bull., 93*, 545-562, 1982.

Dziewonski, A. M., A. Friedman, and J. H. Woodhouse, Centroid-moment tensor solutions for January-March 1983, *Phys. Earth Planet. Inter., 33*, 71-75, 1983a.

Dziewonski, A. M., J. E. Franzen, and J. H. Woodhouse, Centroid-moment tensor solutions for April-June 1983, *Phys. Earth Planet. Inter., 33*, 243-249, 1983.b

Dziewonski, A. M., J. E. Franzen, and J. H. Woodhouse, Centroid-moment tensor solutions for July-September 1983, *Phys. Earth Planet. Inter., 34*, 1-8, 1984a.

Dziewonski, A. M., J. E. Franzen, and J. H. Woodhouse, Centroid-moment tensor solutions for October-December 1983, *Phys. Earth Planet. Inter., 34*, 129-136, 1984b.

Dziewonski, A. M., J. E. Franzen, and J. H. Woodhouse, Centroid-moment tensor solutions for January-March 1984, *Phys. Earth Planet. Inter., 34*, 209-219, 1984c.

Dziewonski, A. M., J. E. Franzen, and J. H. Woodhouse, Centroid-moment tensor solutions for April-June 1984, *Phys. Earth Planet. Inter., 37*, 87-96, 1985a.

Dziewonski, A. M., J. E. Franzen, and J. H. Woodhouse, Centroid-moment tensor solutions for July-September 1984, *Phys. Earth Planet. Inter., 38*, 203-213, 1985b.

Dziewonski, A. M., J. E. Franzen, and J. H. Woodhouse, Centroid-moment tensor solutions for October-December 1984, *Phys. Earth Planet. Inter., 39*, 147-156, 1985c.

Dziewonski, A. M., J. E. Franzen, and J. H. Woodhouse, Centroid-moment tensor solutions for January-March 1985, *Phys. Earth Planet. Inter., 40*, 249-258, 1985d.

Dziewonski, A. M., J. E. Franzen, and J. H. Woodhouse, Centroid-moment tensor solutions for April-June 1985, *Phys. Earth Planet. Inter., 41*, 215-224, 1985e.

Dziewonski, A. M., J. E. Franzen, and J. H. Woodhouse, Centroid-moment tensor solutions for July-September 1985, *Phys. Earth Planet. Inter.*, *42*, 205-214, 1986a.

Dziewonski, A. M., J. E. Franzen, and J. H. Woodhouse, Centroid-moment tensor solutions for October-December 1985, *Phys. Earth Planet. Inter.*, *43*, 185-195, 1986b.

Dziewonski, A. M., G. Ekstrom, Goran, J. E. Franzen, and J. H. Woodhouse, Centroid-moment tensor solutions for January-March 1986, *Phys. Earth Planet. Inter.*, *45*, 1-10, 1987a.

Dziewonski, A. M., G. Ekstrom, Goran, J. E. Franzen, and J. H. Woodhouse, Centroid-moment tensor solutions for April-June 1986, *Phys. Earth Planet. Inter.*, *45*, 229-239, 1987b.

Dziewonski, A. M., G. Ekstrom, J. E. Franzen, and J. H. Woodhouse, Centroid-moment tensor solutions for July-September 1986, *Phys. Earth Planet. Inter.*, *46*, 305-315, 1987c.

Dziewonski, A. M., G. Ekstrom, J. H. Woodhouse, and G. Zwart, Centroid-moment tensor solutions for October-December 1986, *Phys. Earth Planet. Inter.*, *48*, 5-17, 1987d.

Dziewonski, A. M., G. Ekstrom, J. H. Woodhouse, and G. Zwart, Centroid-moment tensor solutions for January-March 1987, *Phys. Earth Planet. Inter.*, *50*, 116-126, 1988a.

Dziewonski, A. M., G. Ekstrom, J. H. Woodhouse, and G. Zwart, Centroid-moment tensor solutions for April-June 1987, *Phys. Earth Planet. Inter.*, *50*, 215-228, 1988b.

Dziewonski, A. M., G. Ekstrom, J. H. Woodhouse, and G. Zwart, Centroid-moment tensor solutions for July-September 1987, *Phys. Earth Planet. Inter.*, *53*, 1-11, 1988c.

Dziewonski, A. M., G. Ekstrom, J. H. Woodhouse, and G. Zwart, Centroid-moment tensor solutions for October-December 1987, *Phys. Earth Planet. Inter.*, *54*, 10-21, 1989a.

Dziewonski, A. M., G. Ekstrom, J. H. Woodhouse, and G. Zwart, Centroid-moment tensor solutions for January-March 1988, *Phys. Earth Planet. Inter.*, *54*, 22-32, 1989b.

Dziewonski, A. M., G. Ekstrom, J. H. Woodhouse, and G. Zwart, Centroid-moment tensor solutions for April-June 1988, *Phys. Earth Planet. Inter.*, *54*, 199-209, 1989c.

Febrer, J. M. , B. Baldis, J. C. Gasco, M. Mamani, and C. Pomposiello, La anomalia geotermica Calchaqui en el noroeste Argentina: Un nuevo proceso geodinamica asociada a la subduccion de la placa de Nazca, *Quinto Congr. Latinoamer. de Geol.*, *3*, 691-703, 1982.

Gephart, J. W., Stress and the direction of slip on fault planes, *Tectonics*, *9*, 845-858, 1990.

Grange, F., P. Cunningham, D. Hatzfeld, S.W. Roecker, P. Molnar, A. Rodrigues, G. Suarez, and L. Ocala, Tectonic implications of the micro-earthquake seismicity and fault plane solutions in southern Peru, *J. Geophys. Res.*, *89*, 6139-6152, 1984.

Hamilton, W., The volcanic central Andes--A modern model for the Cretaceous batholiths and tectonics of western North America, *Oreg. Dep. Geol. Miner. Ind. Bull.*, *65*, 175-184, 1969

Handschumacher, D. W., Post-Eocene plate tectonics of the eastern Pacific, *The geophysics of the Pacific Ocean basin and Its Margin*: *Geophys. Monogr. Ser.*, vol. 19, edited by G. P. Woolard, G. H. Sutton, M. H. Manghnani, and R. Moberly, pp. 17-202, AGU, Washington, D. C., 1976.

Hasegawa, A., and I. S. Sacks, Subduction of the Nazca Plate beneath Peru as determined from seismic observations, *J. Geophys. Res.*, *86*, 4971-4980, 1981.

Isacks, B. L., Uplift of the central Andean plateau and bending of the Bolivian orocline, *J. Geophys. Res.*, *93*, 3211-3231, 1988.

Isacks, B.L. and M. Barazangi, Geometry of Benioff zones: Lateral segmentation and downward bending of the subducted lithosphere, in *Island Arcs, Deep Sea Trenches, and Back Arc Basins, Ewing Ser. vol.* 1, edited by M. Talwani, and W. Pitman, pp. 99-114, AGU, Washington, D.C., 1977.

Isacks, B. L., and P. Molnar, Distribution of stresses in the descending lithosphere from a global survey of focal-mechanism solutions of mantle earthquakes, *Rev. Geophys.*, *9*, 103-174, 1971.

Jordan, T. E., B. L. Isacks, R. W. Allmendinger, J. A. Brewer, V. A. Ramos, and C. J. Ando, Andean tectonics related to geometry of subducted Nazca plate, *Geol. Soc. Am. Bull.*, *94*, 341-361, 1983.

Kadinsky-Cade, K.A., Seismotectonics of the Chile margin and the 1977 Caucete earthquake of western Argentina, Ph.D. dissertation, Cornell Univ., Ithaca, N.Y., 1985.

Kay, S. M., V. Maksaev, R. Moscoso, C. Mpodozis, and C. Nasi, Probing the evolving Andean lithosphere: Mid-late Tertiary magmatism in Chile (29°-30°30'S) over the modern zone of subhorizontal subduction, *J. Geophys. Res.*, *92*, 6173-6189, 1987.

Kelleher, J. and W. McCann, Buoyant zones, great earthquakes and unstable boundaries of subduction, *J. Geophys. Res.*, *81*, 4885-4896, 1976.

Knox, W. J., B. Coira, and S. M. Kay, Evidencias geochimicas sobre el origen de rocas volcanicas maficas cuartarias en la Puna, Argentina, *X Congr. Geol. Argen.*, *4*, 341-343, 1987.

Kono, M., Y. Takahashi, and Y. Fukao, Earthquakes in the subducting slab beneath northern Chile: A double-seismic zone ?, *Tectonophysics*, *112*, 112-225, 1985.

Lowrie, A., and R. Hey, Geological and geophysical variations along the western margin of Chile near lat. 33°S to 36°S and their relation to Nazca plate subduction; in *Mem. Geol. Soc. Am. 154*, 741-754, 1981.

Lyon-Caen, H., P. Molnar, and G. Suárez, Gravity anomalies and flexure of the Brazilian Shield beneath the Bolivian Andes, *Earth Planet. Sci. Lett.*, *75*, 81-92, 1985.

Mammerickx, J., and S. M. Smith, Bathymetry of the Southeast Pacific, *Geol. Soc. Am. Map Ser.* folio MC-26, Geol. Soc. Am., Boulder, Colo., 1978.

Molnar, P., D. Freedman, and J.S.F. Shih, Length of intermediate and deep seismic zones and temperatures in downgoing slabs of lithosphere, *Geophys. J. R. Astron. Soc.*, *56*, 41-54, 1979.

Noble, D.C. and E.H. McKee, Spatial distribution of earthquakes and subduction of the Nazca plate beneath South America: Comment, *Geology*, *5*, 576-578, 1977.

Pilger, R. H., Jr., Plate reconstructions, aseismic ridges, and low-angle subduction beneath the Andes, *Geol. Soc. Am. Bulletin*, *92*, 448-456, 1981.

Roeder, D., Andean-age structure of the eastern cordillera (province of La Paz, Bolivia), *Tectonics*, *7*, 23-29, 1988.

Santo, T., Characteristics of seismicity in South America, *Bull. Earthquake Res. Instit. Univ. Tokyo* , *47*, 635, 1969.

Schneider, J. F., and I. S. Sacks, Stress in the contorted Nazca plate beneath southern Peru from local earthquakes, *J. Geophys. Res.*, *92*, 13,887-13,902, 1987.

Sheffels, B. M., Structural constraints on crustal shortening in the Bolivian Andes, Ph. D. dissertation, Mass. Inst. Technol., Cambridge, Mass., 1988.

Simkin, T., L. Siebert, L. McClelland, D. Bridge, C. Newhall, and J. H. Latter, *Volcanoes of the world* (Smithsonian Institute), 223 pp., Hutchenson Ross, Stroudsburg, Pa., 1981.

Smalley, R. F., and B. L. Isacks, A high resolution local network study of the Nazca Plate Wadati-Benioff Zone under western Argentina, *J. Geophys. Res.*, *92*, 13,093-13,912, 1987.

Stauder, W., Mechanisms and spatial distribution of Chilean earthquakes with relation to subduction of the oceanic plate, *J. Geophys. Res.*, *78*, 5033-5061, 1973.

Stauder, W., Subduction of the Nazca plate under Peru as evidenced by focal mechanisms and by seismicity, *J. Geophys. Res.*, *80*, 1053-1064, 1975.

Sykes, L., and D. Hayes, Seismicity and tectonics of South America and adjacent oceanic areas, *Geol. Soc. Am. Programs*, Cordilleran section, *3*, 206, 1971.

Turner, J. C. M., and V. Mendez, Puna, in *Segundo Simposio de Geologia Regional*; Academia Nacional de Ciencias, Cordoba, vol. 1, 1979.

Vogt, P. R., A. Lowrie, D.R. Bracey, and R.H. Rey, Subduction of aseismic oceanic ridges: Effects on slope, seismicity, and other characteristics of consuming plate boundaries, *Geol. Soc. Am. Spec. Pap. 172*, 59 pp., 1976.

Yamaoka, K.Y., Y. Fukao, and M. Kumazawa, Spherical shell tectonics: Effects of sphericity and inextensibility on the geometry of the descending lithosphere, *Rev. Geophys.*, *24*, 27-55, 1986.

**T. Cahill, Engineering Tectonics, P.A., P.O. Box 4798, Winston-Salem, NC 27115.**

**B.L. Isacks, Institute for the Study of Continents and Department of Geological Sciences, Cornell University, Ithaca, NY 14853.**

(Received June 5, 1991;
revised February 13, 1992;
accepted February 24, 1992.)